Volume 3

Chapter 14

https://doi.org/10.32685/pub.esp.37.2019.14
Published online 5 June 2020

New Contributions to Knowledge about the Chocó–Panamá Arc in Colombia, Including a New Segment South of Colombia

Gilberto ZAPATA–GARCÍA[1]* and Gabriel RODRÍGUEZ–GARCÍA[2]

1 gilbertozapatag@yahoo.com
Servicio Geológico Colombiano
Dirección de Geociencias Básicas
Grupo de Estudios Geológicos Especiales
Calle 24A n.° 50A–31
Bello, Antioquia, Colombia

2 grodriguez@sgc.gov.co
Servicio Geológico Colombiano
Dirección de Geociencias Básicas
Grupo de Estudios Geológicos Especiales
Calle 75 n.° 79A–51
Medellín, Colombia

* Corresponding author

Abstract Geological mapping and petrographic, lithogeochemical, and geochronologic analyses show that the volcanic rocks and plutons that constitute the Chocó–Panamá Arc are segmented into three sectors: North (Santa Cecilia–La Equis Complex and Acandí Batholith); Central (Santa Cecilia–La Equis Complex and Mandé Batholith); and South (Timbiquí Formation and Napi Tonalite). In this study we include the South segment, which was not considered part of the Chocó–Panamá Arc in previous studies. This magmatism occurred during the Eocene (Ypresian Stage). The rocks of the Santa Cecilia–La Equis Complex and the Timbiquí Formation are constituted of basalts and andesites interbedded with pyroclastic facies of tuffs and agglomerates. These are subalkaline and plot in the tholeiitic–normal calc–alkaline series. The Acandí Batholith presents two granitic facies: the main facies is a tonalite–granodiorite–quartz diorite, and the secondary is a gabbro–diorite, located towards the edges of the intrusive. Both are metaluminous subalkaline, low potassium tholeiitic, and medium potassium calc–alkaline. The Mandé Batholith is constituted by tonalites and quartz diorites, with porphyritic facies near the Santa Cecilia–La Equis Complex. These rocks are subalkaline within the tholeiitic series. The Chocó–Panamá Arc in the Central segment is limited by the recent sediments of the Atrato River, on the west, and by tectonic boundaries such as the Dabeiba–Pueblo Rico and the Amurrapá Faults, on the east, which separate this block from the accreted oceanic sequences with oceanic plateau geochemical affinities. The South segment is a tectonic block in contact with the Dagua Structural Complex, bounded by Piedramadura Fault. According to the ages obtained in this study, and by other authors using K–Ar, Ar–Ar, and U–Pb dating, the Chocó–Panamá Arc magmatism in Colombia occurred between 56.5 and 37 Ma.

Keywords: *northwest South America, Western Cordillera, lithogeochemistry, geochronology.*

Resumen La cartografía geológica y los análisis petrográficos, litogeoquímicos y geocronológicos muestran que las vulcanitas y plutones que conforman el Arco Chocó–Panamá comprenden tres segmentos: Norte (Complejo Santa Cecilia–La Equis y Batolito de Acandí), Central (Complejo Santa Cecilia–La Equis y Batolito de Mandé) y Sur (Formación Timbiquí y Tonalita de Napi). En este trabajo incluimos el segmento Sur, que en estudios anteriores no se consideró como parte del Arco Chocó–Panamá. Este magmatismo ocurrió durante el Eoceno (Ypresiano). Las rocas del Complejo Santa Cecilia–La Equis y de la Formación Timbiquí son basaltos y andesitas intercaladas con

Supplementary Information:
S: https://www2.sgc.gov.co/LibroGeologiaColombia/tgc/sgcpubesp37201914s.pdf

Citation: Zapata–García, G. & Rodríguez–García, G. 2020. New contributions to the knowledge about the Chocó–Panamá Arc in Colombia, including a new segment south of Colombia. In: Gómez, J. & Mateus–Zabala, D. (editors), The Geology of Colombia, Volume 3 Paleogene – Neogene. Servicio Geológico Colombiano, Publicaciones Geológicas Especiales 37, p. 417–450. Bogotá. https://doi.org/10.32685/pub.esp.37.2019.14

facies piroclásticas de tobas y aglomerados. Estas rocas son subalcalinas y se grafican en los campos de las series toleítica y calcoalcalina normales. El Batolito de Acandí presenta dos facies graníticas: una principal tonalita–granodiorita–cuarzodiorita y la segunda gabro–diorita, que se encuentra hacia los bordes del cuerpo intrusivo. Ambas facies son subalcalinas metaluminosas de la serie toleítica baja en potasio y calcoalcalina con contenido medio de potasio. El Batolito de Mandé está constituido por tonalitas y cuarzodioritas, con facies porfídicas hacia los contactos con el Complejo Santa Cecilia–La Equis. Estas rocas son subalcalinas de la serie toleítica. En el segmento Central, el Arco Chocó–Panamá está limitado, al occidente, por sedimentos recientes del río Atrato y, al oriente, por límites tectónicos como las fallas de Dabeiba–Pueblo Rico y Amurrapá, que separan este bloque de las secuencias oceánicas acrecionadas con afinidades geoquímicas de meseta oceánica (*plateau*). El segmento Sur es un bloque tectónico en contacto con el Complejo Estructural Dagua, limitado por la Falla de Piedramadura. De acuerdo con las edades obtenidas en este estudio, y por otros autores que usaron los métodos K–Ar, Ar–Ar y U–Pb, el magmatismo del Arco Chocó–Panamá en Colombia ocurrió entre 56,5 y 37 Ma.

Palabras clave: *noroccidente de Suramérica, cordillera Occidental, litogeoquímica, geocronología.*

1. Introduction

We present new petrographic, lithogeochemical, and geochronological data for the Chocó–Panamá Arc in Colombia. A new block is included, named the South segment (Figure 1), which had not been mentioned in previous studies.

The Chocó–Panamá Arc is exposed west of the Colombian Western Cordillera and is a Late Cretaceous – Eocene plutonic–volcanic arc of tholeiitic to calc–alkaline affinity, consisting of basaltic and andesitic lavas that are associated with plutons of dominantly tonalitic composition (Duque–Caro, 1990; Pindell, 1993).

Previous geological studies have used different names to describe the blocks that compose the Colombian northwestern Andes, including units from different geotectonic environments that lack clear spatiotemporal relationships. Etayo–Serna et al. (1983) grouped the Santa Cecilia–La Equis Complex and the Mandé Batholith in the Cañasgordas Terrane and the Timbiquí Formation and the Napi Tonalite in the Dagua Terrane. Restrepo & Toussaint (1989) defined the Cuna Terrane and included the Mandé Batholith. Duque–Caro (1990) grouped the Dabeiba and Baudó Arcs, the Istmina deformed zone, and the Atrato–Chucunaque Basins in the Chocó Block. Salazar et al. (1991) suggested grouping the Santa Cecilia and La Equis Formations (Calle & Salinas, 1986) and the Mandé Batholith into the Santa Cecilia–La Equis Complex. González (2001) proposed that the Santa Cecilia–La Equis Complex should include only the basic volcanic rocks, excluding the intrusive bodies (e.g., the Mandé Batholith). In this study, the Chocó–Panamá Arc is considered a block outside the Cuna Terrane.

This research reviews the current knowledge about the Chocó–Panamá Arc, describes its different segments, and shows the petrographic, lithogeochemical, and geochronological characteristics of the three segments of the arc: (1) North: Santa Cecilia–La Equis Complex and Acandí Batholith; (2) Central: Santa Cecilia–La Equis Complex and Mandé Batholith; and (3) South: Timbiquí Formation and Napi Tonalite (Figure 1). Data from Panamá to the border with Ecuador are compared and integrated, and new petrographic, lithogeochemical, and Ar–Ar radiometric data are presented in order to define the characteristics of the Chocó–Panamá Arc.

2. Geological Framework

The interaction of the Nazca, Cocos, Caribbean, and South American Plates has shaped the geological configuration of western Colombia. Buchs et al. (2010), Barat et al. (2014), Molnar & Sykes (1969), Montes et al. (2012), Pindell (1993), and Pindell & Kennan (2009) consider that the triple junction among the plates began in the Campanian and lasted until the early Oligocene, marked by the termination of magmatism in the Chocó–Panamá Block.

The Western Cordillera constitutes accreted allochthonous terranes composed of Upper Cretaceous – Eocene volcanic and plutonic rocks, which originally formed in oceanic plateau and oceanic arc environments and collided with the South American continental margin (Echeverri et al., 2015; Kerr et al., 1997; Montes et al., 2012; Pindell et al., 1988, 2005; Pindell & Kennan, 2009; Rodríguez & Zapata, 2013; Toussaint, 1996; Villagómez et al., 2011).

The Chocó–Panamá Arc is exposed along the western foothills of the Western Cordillera and is bounded by recent sediments to the west and regional fault systems to the east, including the Dabeiba–Pueblo Rico Fault System. The latter

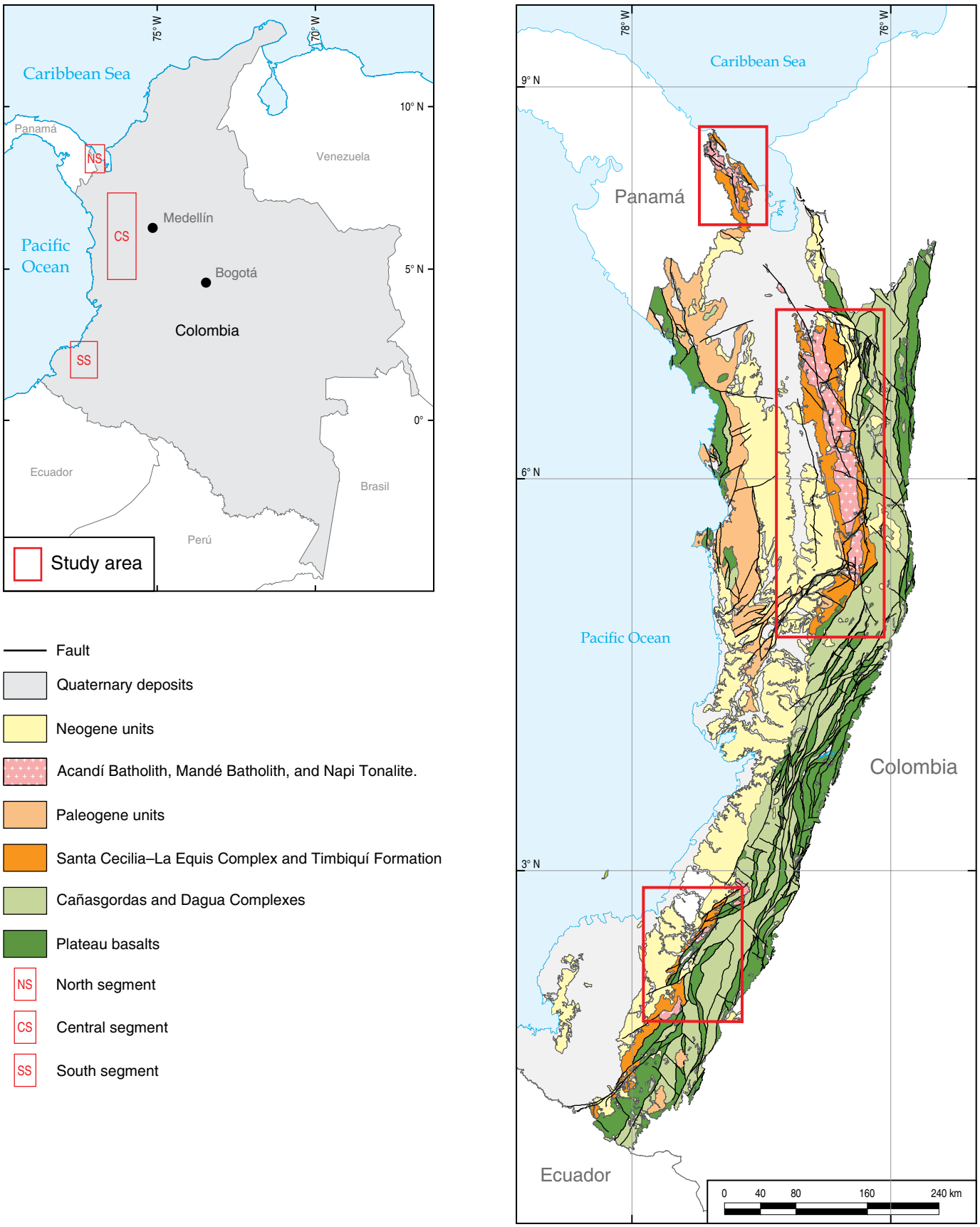

Figure 1. Chocó–Panamá Arc segments in Colombia. Modified from Gómez et al. (2015a).

fault serves as the regional fundamental boundary with the Cretaceous volcanic rocks of the Cañasgordas Group.

In Colombia, the Chocó–Panamá Arc basement is composed of rocks with plateau geochemical affinities (this study), similar to the basement rocks in Panamá (Buchs et al., 2010; Montes et al., 2012). The basaltic rocks with oceanic affinity have been named the Diabasic Group (Barrero, 1979; Nelson, 1962) and/or Volcanic Formation (Aspden, 1984) to the south of the cordillera, La Trinidad Basalts in the central zone (Parra, 1983), and the Barroso Formation to the north (Álvarez & González, 1978). In this work, the nomenclature proposed by Rodríguez & Arango (2013), in which the San José de Urama Diabase (oceanic crust) is separated from the Barroso Formation (arc volcanic rocks), is used.

Oceanic plateau sequences of the Western Cordillera are generally considered Late Cretaceous (ca. 90 Ma) in age (e.g., Kerr et al., 1997; Nivia, 2001; Rodríguez & Arango, 2013; Villagómez et al., 2011; Weber et al., 2015), but recent regional studies suggest a much broader, still poorly defined age range (Kerr et al., 1997; Nivia, 1996, 1998, 2001; Villagómez et al., 2011; Rodríguez & Arango, 2013; Weber et al., 2015). Additionally, El Palmar Gabbro (with oceanic plateau geochemical affinity) was dated at 100 Ma (Villagómez, 2010), and Whattam & Stern (2015) compiled the Ar–Ar and U–Pb ages published by Kerr et al. (1997), Villagómez (2010), and Serrano et al. (2011), which range from 100 to 81 Ma, suggesting the presence of older rocks in the Western Cordillera.

On top of the basalts with oceanic affinity (plateau), a tholeiitic to calc–alkaline arc was emplaced (the Barroso–Sabanalarga Arc) (Rodríguez & Arango, 2013), constituting basalts, andesites, tuffs, and volcanic breccias, which are intruded by gabbroic to tonalitic plutons with ages between 103 and 83 Ma (Correa et al., 2017; Rodríguez et al., 2012; Rodríguez & Arango, 2013). According to Zapata–Villada et al. (2017), the accretion of the oceanic units to the South American continent occurred after 86 Ma.

Upper Cretaceous turbiditic sedimentary sequences composed of discontinuous fault–bounded belts of stretched rhomboid–shaped assemblages of mudstones, wackes, sandstones, cherts, conglomerates, limestones, tuffs, and volcanic breccias with superimposed dynamic deformation were deposited atop this basement. These rocks are the Dagua Complex in the south (Nivia, 2001) and the Penderisco Formation in the north (Álvarez & González, 1978).

The Chocó–Panamá Arc in Colombia is composed of basaltic to andesitic volcanic rocks and intermediate plutonic rocks, which are divided into three segments.

The Northern segment includes La Iguana, Tripogadí, and Darién highlands in Colombia, extending into Panamá and forming the oroclinal curvature in the San Blas Range. The areas present volcanic rocks of basic to intermediate composition (the Santa Cecilia–La Equis Complex) exposed in two elongated belts parallel to the cordillera, including the Acandí Batholith (Figure 2).

The Central segment extends from the Aguasal–Amurrapá Fault in the south (Arboleda et al., 2009) to the alluvial sediments of the Atrato River in the north and west, bordering the plateau basalts (Cañasgordas Block) along the Dabeiba–Pueblo Rico Fault (Rodríguez et al., 2010a) in the east. This segment is composed of the Santa Cecilia–La Equis Complex, which is exposed as strips on both sides of the Mandé Batholith (Figure 3). These units were intruded in the Miocene by arc plutons with ages between 12 and 9 Ma (Nudillales Monzonite, Carauta Monzodiorite, and Valle de Pérdidas Quartz diorite) and volcanic rocks of alkaline affinity related to El Botón Arc (Rodríguez & Zapata, 2012; Zapata & Rodríguez, 2011).

The southern segment is a tectonic block exposed in Guapi (Cauca Department) that buttresses the Dagua Structural Complex along the Piedramadura Fault on the southwestern slope of the cordillera (Geología Regional y Prospección Ltd., 2014a, 2014b, 2014c). This segment includes the middle Eocene – Oligocene volcano–sedimentary rocks from the Timbiquí Formation (Annells et al., 1988), exposed in a belt that trends northeast, which is intruded by the Napi Tonalite and the Munchica Gabbro (Figure 4). The volcanic rocks of the Timbiquí Formation have been considered an andesitic sequence of subaerial volcanism possibly formed in an area near a continental margin in the emerging part of an arc (Geología Regional y Prospección Ltd., 2014b, 2014c).

3. Materials and Methods

Data from several regional mapping projects associated with contracts signed by the Servicio Geológico Colombiano (SGC) and the Agencia Nacional de Hidrocarburos (ANH) and from published articles were compiled to characterize the origins of the three segments that constitute the Chocó–Panamá Arc. Thin sections from the Central segment were revised, databases were organized by lithological units, and samples were georeferenced, including petrographic, geochemical, and geochronological descriptions. The analysis and interpretation of the results were conducted for each unit and segment, excluding the alkaline samples from El Botón Arc. Finally, the data supporting this chapter are presented in Tables 1 to 12 of the Supplementary Information.

3.1. Petrography

New petrographic analyses, data from previous SGC projects and maps from plates 319, 341, and 363 of the ANH (Geología Regional y Prospección Ltd., 2014a, 2014b, 2014c) were considered.

The petrographic description of the Santa Cecilia–La Equis Complex in the North and Central segments was based on 302 petrographic analyses: 24 from the North segment by Rodríguez et al. (2010b) and 279 from the Central segment, including 55 from Buchely et al. (2009). To describe the Acandí Batholith, 51 thin sections from Rodríguez et al. (2010b) were reanalyzed.

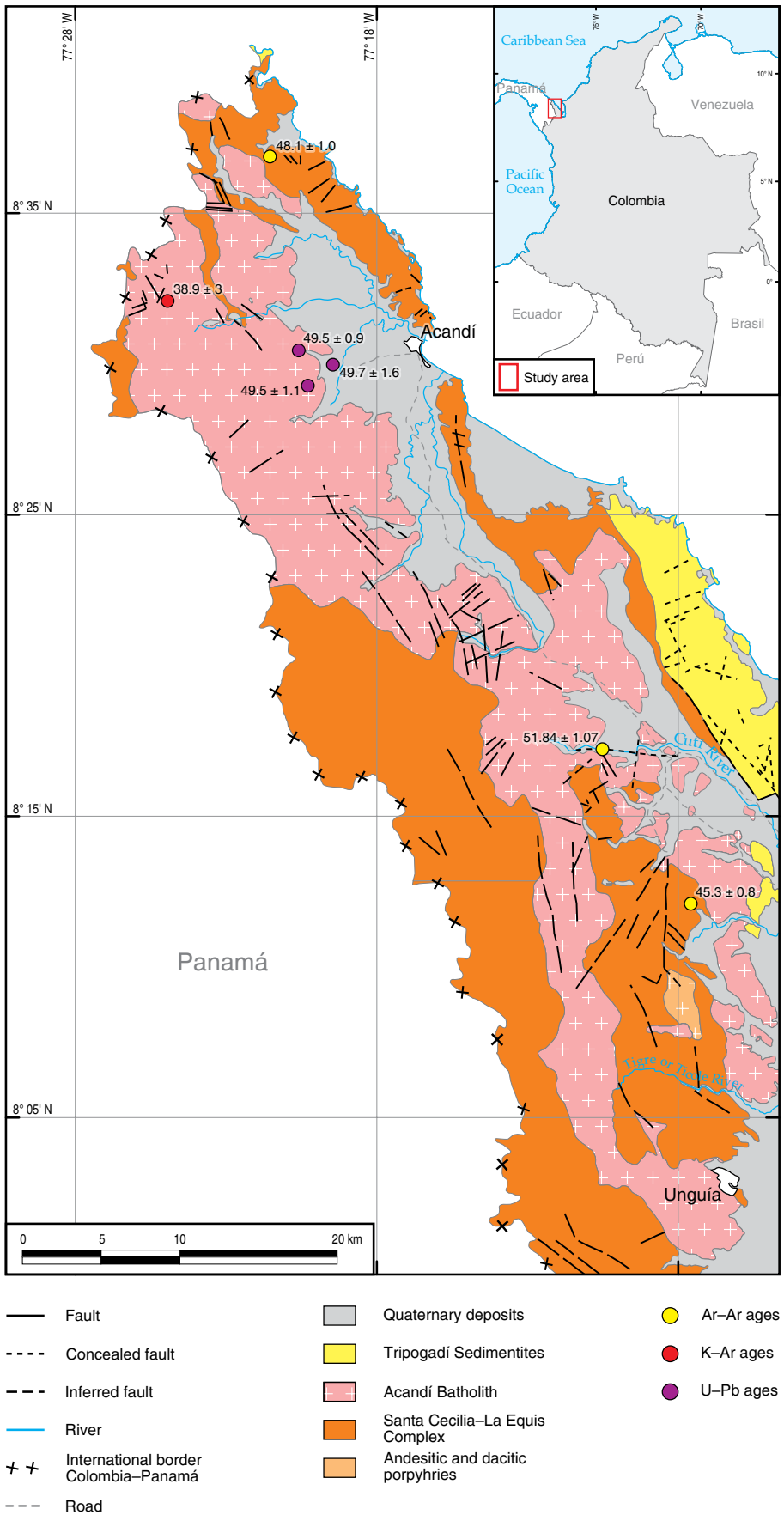

Figure 2. Geology and dates of the Chocó–Panamá Arc, North segment. Modified from Rodríguez et al. (2010b).

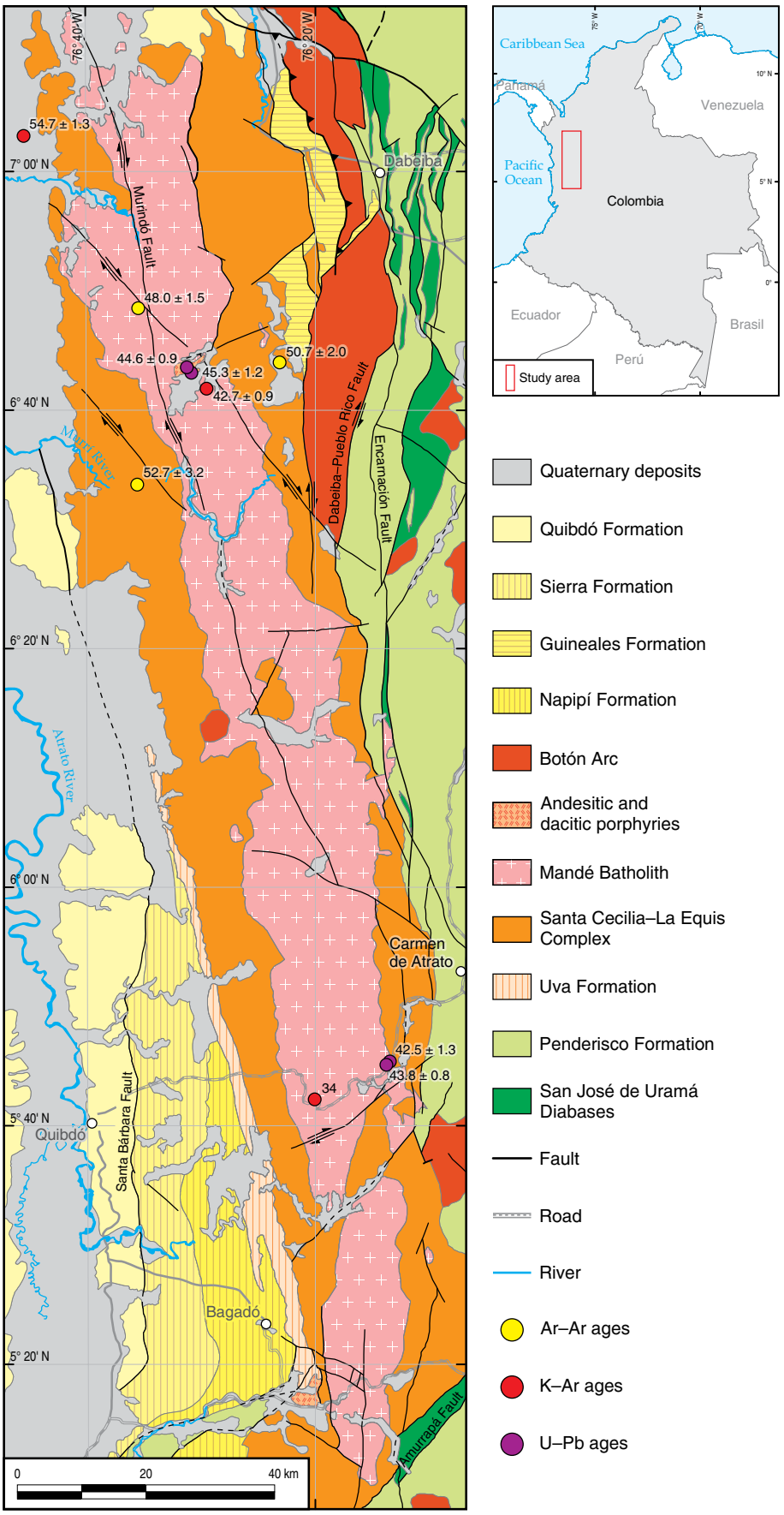

Figure 3. Geology and dates of the Chocó–Panamá Arc, Central segment. Modified from Gómez et al. (2015a).

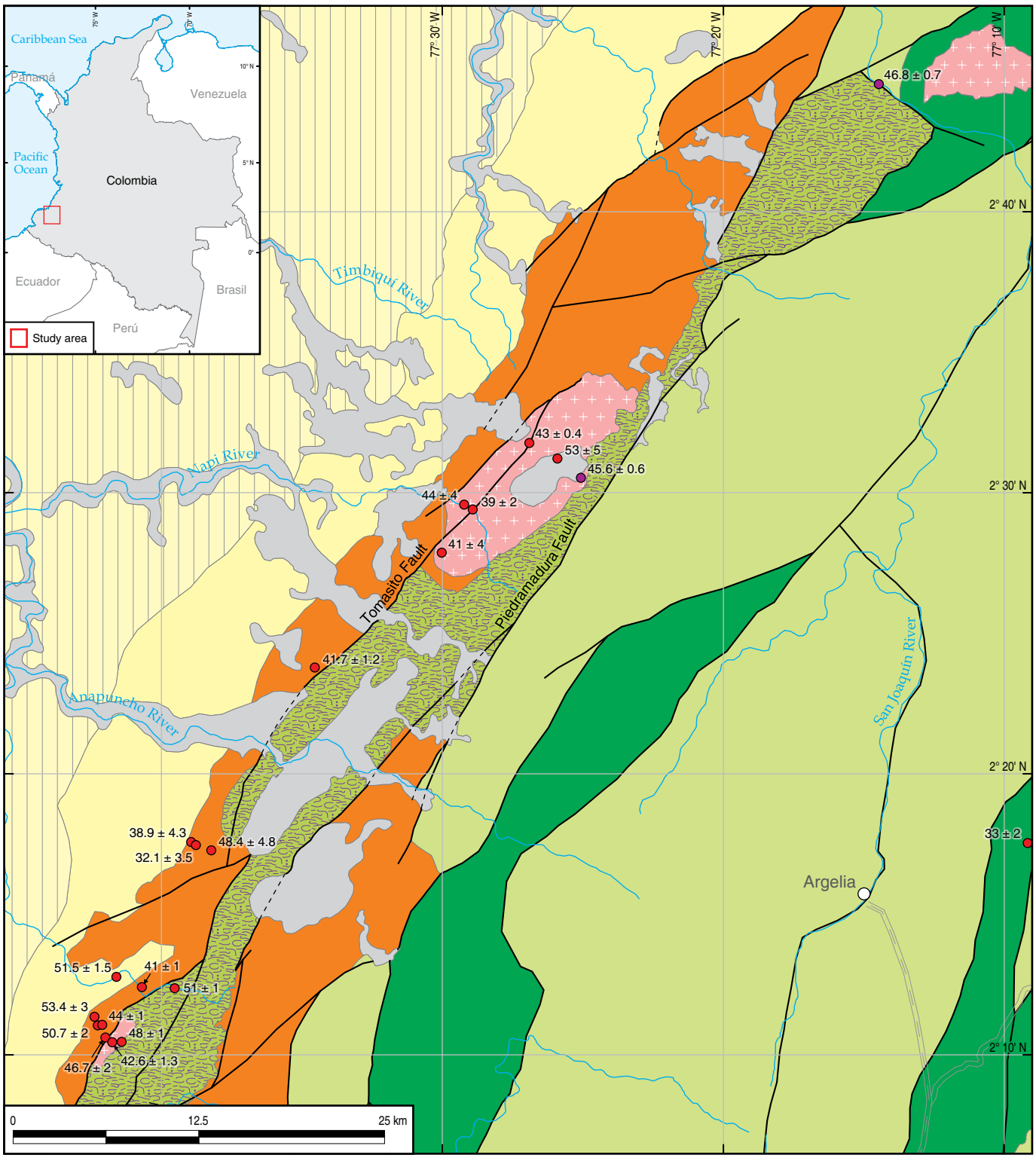

Figure 4. Geology and dates of the Chocó–Panamá Arc, South segment. Modified from Gómez et al. (2015a).

To describe the Mandé Batholith in the Central segment, 266 thin sections from different SGC projects were studied, most of which were reanalyzed in this research to complete the mineralogical descriptions and perform modal counts. To describe the Timbiquí Formation and Napi Tonalite (South segment), data from Geología Regional y Prospección Ltd. (2014a, 2014b, 2014c) were considered. The data include descriptions of 21 thin sections of volcanic rocks and 16 analyses of the Napi Tonalite and other associated intrusive bodies.

3.2. Whole–Rock Geochemistry

Major and minor oxides, trace elements, and rare earth elements were analyzed by ActLabs, Canadá, using 100 g of sample and ICP–MS (inductively coupled plasma mass spectrometry) methodology with lithium metaborate–tetraborate complete fusion. The samples were pulverized to –200 mesh in a noncontaminating mill. Some samples from Salazar et al. (2005) were reanalyzed by ICP–MS for 62 major and trace elements.

To interpret the major oxides and classify the rocks, values were recalculated on an anhydrous basis and were graphed in the TAS diagrams (total alkali–silica diagram) of Le Bas et al. (1986) and Middlemost (1985) for volcanic and intrusive rocks, respectively, as recommended by Le Maitre et al. (2002).

3.3. Geochronology

Four samples were analyzed by ActLabs, Canadá with the Ar–Ar step heating dating method. The rocks were prepared in a noncontaminating mill at –200 mesh. The samples were wrapped in aluminum foil and loaded into a vacuum–sealed quartz vessel with K and Ca salts and LP–6 biotite packs, used as a flux monitor, interspersed with the samples. Samples were irradiated in the nuclear reactor for 48 hours. The flux monitors were placed every two samples, allowing the exact determination of the flow gradients inside the tube. After the flow monitors were run, J values were calculated for each sample using the gradient of the flow tested. The LP–6 biotite featured an estimated age of 128.1 Ma. The neutron gradient reading did not exceed 0.5% of the sample size. The isotope composition of Ar was calculated on a Micromass 5400 static mass spectrometer. The 1200 °C target reading of ^{40}Ar did not exceed $n*10^{-10}$ cc STP. The plateau ages from the age ranges integrated by several gas fractions released by the gradual heating of samples represented more than 50% of the ^{39}Ar released by the sample, and the released fractions were within a confidence level of 1σ.

4. Results

This section presents the petrography, lithogeochemistry, and radiometric dating results for the Santa Cecilia–La Equis Complex, Acandí Batholith, Mandé Batholith, Timbiquí Formation, and Napi Tonalite.

4.1. Petrography of Volcanic Rocks

4.1.1. Santa Cecilia–La Equis Complex

This complex includes lavas petrographically classified as porphyritic augite basalts, two–pyroxene basalts, and andesitic basalts with porphyritic, glomeroporphyritic, and amygdaloidal textures. The rock matrix (30–75 %) is holocrystalline to hyalocrystalline, microlitic, and sometimes fluidal and trachitic. The phenocrysts and microcrysts are augite, plagioclase (labradorite), and occasionally olivine. Amygdules are filled with quartz, chalcedony, zeolites, calcite, epidote, and chlorite in both aggregates and crystals. The two–pyroxene basalts contain orthopyroxene and clinopyroxene. The accessory minerals are opaque minerals and sphene.

The pyroclastic rocks are basaltic breccias and tuffs. The matrix presents poor selection with sizes ranging from fine ash to lapilli. The lithic fragments are porphyritic, amygdaloidal, and augite basalts and tuffs. Crystals include augite, calcium plagioclase, and volcanic glass.

Within the northern Santa Cecilia–La Equis Complex, some thin sections are classified as basalts with inequigranular–hypidiomorphic textures. The crystals show intergranular, intersertal and subophitic adjustments and include plagioclase, pyroxene, and accessory minerals such as opaques, sphene, and epidote. These crystals possibly correspond to xenoliths from older basement (plateau). Most rocks of the Santa Cecilia–La Equis Complex in the Central segment (>75%) are basalts and andesites (Figure 5).

4.1.2. Timbiquí Formation

This unit is exposed in the South segment, forming two NW–oriented belts adjacent to the Napi Tonalite and the Guapi ultramafic rocks. The Timbiquí Formation is composed of pyroclastic rocks (lithic, crystalline, and vitric tuffs with basalt and andesite fragments), basaltic andesites, and andesites, interbedded with siltstones and black cherts intervals. The flows show porphyritic and glomeroporphyritic textures with plagioclase, augite, olivine, and hornblende phenocrysts. The matrix is hyalocrystalline to vitreous with fluidal texture, with plagioclase microliths, hornblende, and pyroxene. Amygdules are filled with chlorite, epidote, and quartz.

In the Timbiquí Formation, all of the samples are basalts and andesites (Figure 5). In the QAFP diagram, the Timbiquí Formation rocks are restricted to a single point because of the total lack of quartz and feldspar in the petrographic analysis.

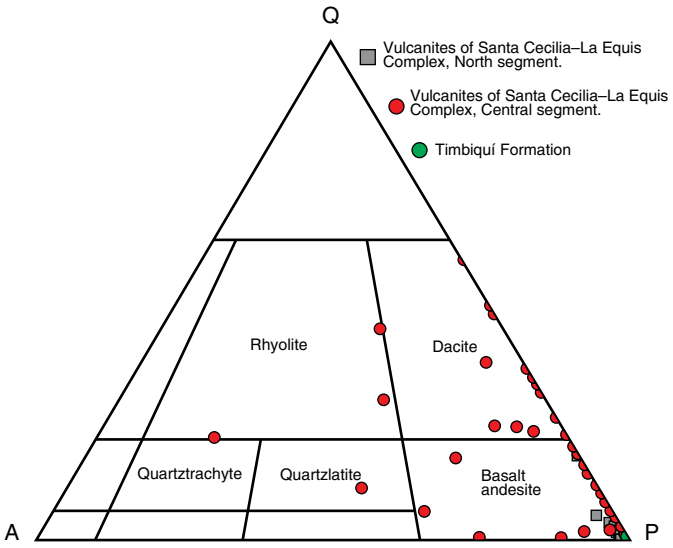

Figure 5. Modal compositions of volcanic rocks from the Chocó–Panamá Arc (Streckeisen, 1979). Vulcanites of the Santa Cecilia–La Equis Complex North segment (gray), Central segment (red), and Timbiquí Formation (green).

4.2. Petrography of Plutonic Rocks

The plutonic rocks are black and gray and white speckled, composed of plagioclase, quartz, biotite, hornblende, and K–feldspar, equigranular to inequigranular, and fine to medium grained. These rocks are cut by dikes and minor porphyry units. Plutonic rocks intrude the volcanic rocks and produce thermal metamorphism in the interaction zone.

4.2.1. Acandí Batholith

The batholith shows wide lithological variation with tonalite–granodiorite–monzogranite–quartz diorite facies (Figure 6), as well as gabbro–diorite and dikes. Tonalite is the most common rock type, with allotriomorphic, subidiomorphic, hypidiomorphic, granular, and inequigranular textures. Tonalites present quartz, plagioclase (oligoclase and andesine), orthoclase, hornblende, and biotite. The accessory minerals are opaque minerals, apatite, sphene, and occasionally zircon and rutile. The gabbro–diorite facies includes diorite, microdiorite, gabbro, hornblendic gabbro, microgabbro, gabbronorite, and monzogabbro. These rocks are intruded by stocks and andesite and porphyritic dacite dikes (Rodríguez et al., 2010a).

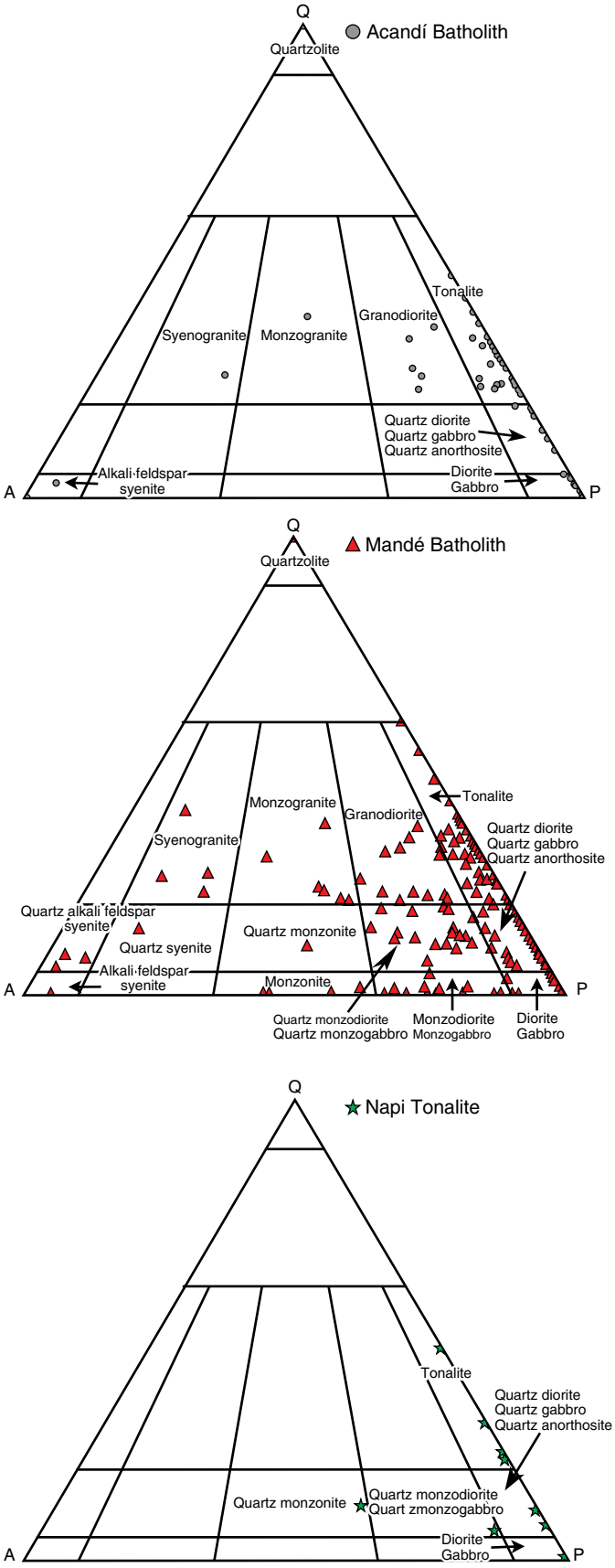

Figure 6. Modal compositions of plutonic rocks from the Chocó–Panamá Arc (Streckeisen, 1976). Acandí Batholith (gray), Mandé Batholith (red), and Napi Tonalite (green).

4.2.2. Mandé Batholith

This intrusive unit is of diverse lithological composition, including tonalite and quartz diorite with subordinate granodiorite (Figure 6). The gabbro–diorite facies is most common near the eastern boundary, in contact with the Santa Cecilia–La Equis Complex. Porphyry units intrude the plutonic rocks and include disseminated Cu–Au and Cu–Mo mineralization zones (Pantanos–Pegadorcito, Ramírez et al., 1979; Murindó, Guarín & Álvarez, 1975; and Acandí, Álvarez & Parra, 1979; Sillitoe et al., 1982). The contact between the granitoid unit and the volcanic rocks of the Barroso Formation (basalts and andesites) is intrusive and develops hornfels and intrusive breccia zones (González & Londoño, 2002).

The Mandé Batholith presents subidiomorphic and hypidiomorphic, inequigranular to granular, poikilitic and graphic textures. Plagioclase (andesine) is the prevailing mineral, followed by quartz, hornblende, alkali feldspar, and biotite. The accessory minerals include apatite, zircon, sphene, and opaque minerals. The alteration minerals include chlorite, epidote, sericite, saussurite, and kaolinite.

The porphyries that intrude the Mandé Batholith vary from andesitic to dacitic. The andesitic porphyries feature hornblende and plagioclase phenocrysts in a crystalline matrix of feldspar and fine quartz. As an accessory mineral, bipyramidal quartz with apatite inclusions is present, featuring thin reaction crowns at the contacts with the matrix. The porphyritic dacites are composed of bipyramidal quartz phenocrysts with corroded edges, plus plagioclase and chlorite produced by hydrothermal alteration. The matrix is holocrystalline, aphanitic, and composed of feldspar and quartz.

4.2.3. Napi Tonalite

This unit is composed of quartz diorite, tonalite, diorite, and gabbro (Figure 6). It includes plagioclase (oligoclase and andesine), quartz, potassium feldspar, hornblende, and biotite, as well as opaque minerals, sphene, zircon, and apatite as accessory minerals. The alteration minerals are chlorite, epidote, sericite, clay minerals, and calcite.

The gabbroic facies rocks are classified as pyroxene–hornblende melanogabbro, leucogabbro, quartz gabbro, and pyroxene–hornblende gabbro.

4.3. Geochemistry of Volcanic Rocks

The Santa Cecilia–La Equis Complex, in the North segment, presents LOI values between 2 and 5.06%, suggesting moderate alteration of the rocks. In the Central segment, most of the rocks have LOI <3%, which is indicative of low alteration, except for samples 80588 (LOI = 4.04%), 119082 (LOI = 6.24%), 701803 (LOI = 5.09%), and 702760 (LOI = 4.48%), which indicate alteration. The rocks of the Timbiquí Formation have LOI <3%, except for samples APO–0036–P (LOI = 6.2%), APO–0065–LT (LOI = 4%), CDG–0262P (LOI = 5.3%), and CDG–0267P (LOI = 3.8%), which are indicative of moderate to high alteration. Additionally, in the Hughes diagram (Hughes, 1972), some samples from the Santa Cecilia–La Equis Complex (North segment) and the Timbiquí Formation (South segment) plot in the spilite field, indicating albitization probably due to contact with seawater during the crystallization of the rocks; three samples from the Santa Cecilia–La Equis Complex plot within the field of potassic alteration (706413, 703017, 702633) (Figure 7a).

The Santa Cecilia–La Equis Complex in the North and Central segments presents SiO_2 values between 46 and 60%, low K_2O contents between 0.07 and 3.1% (with most samples between 0.5 and 1.5%), TiO_2 <1%, and MgO between 2.65 and 10.99%. MgO, CaO, and Fe_2O_3 decrease, and Na_2O increases as SiO_2 increases. The remaining oxides show wide dispersions without defined tendencies. The Timbiquí Formation in the South segment presents SiO_2 contents between 49.17 and 65.75% and low values of TiO_2 <1%, K_2O <1.4, and MgO <9.64, and other oxide values are similar to those of the Santa Cecilia–La Equis Complex (Table 1). The chemical classification of the rocks matches the petrographic classification in the three segments, varying between basalts and dacites, but mostly andesites and basaltic andesites (Figure 7a, 7b).

The Santa Cecilia–La Equis Complex and the Timbiquí Formation are subalkaline and plot in the tholeiitic and normal calc–alkaline series (Figures 7c, 7f). These rocks are mostly basic to intermediate and metaluminous, with A/CNK ratios between 0.5 and 1.2 and A/NK values between 1.1 and 4.5. Some are peraluminous (Figure 7d), as suggested by the high values of loss on ignition (LOI) and the alteration diagram (Figure 7a; Table 1); however, not all are altered, and some could have been formed due to sediment contamination, hydrous melting of mafic rocks or melting of pelitic or semipelitic rocks.

In the Y vs. Sr/Y diagram, most of the volcanic samples of the Santa Cecilia–La Equis Complex and the Timbiquí Formation plot in the field of normal arc rocks, with only very few data in the adakitic series (Figure 7e).

The Santa Cecilia–La Equis Complex and the Timbiquí Formation present trace element patterns with negative Nb and Zr anomalies and positive Cs, Th, Sr, Ba, and Pb anomalies, characteristic of magma generated in arc environments (Pearce, 1996; Pearce et al., 1984). These results show a progressive decrease in LILE toward HFSE (Figure 8). The Nb anomalies are greater in the Santa Cecilia–La Equis Complex rocks than in the Timbiquí Formation. The rare earth element (REE) patterns normalized to the Nakamura chondrite (Nakamura, 1974) are subparallel in the rocks of the three segments, with negative slopes and patterns that are comparable to those of rocks derived from subduction environments above the associated sub-

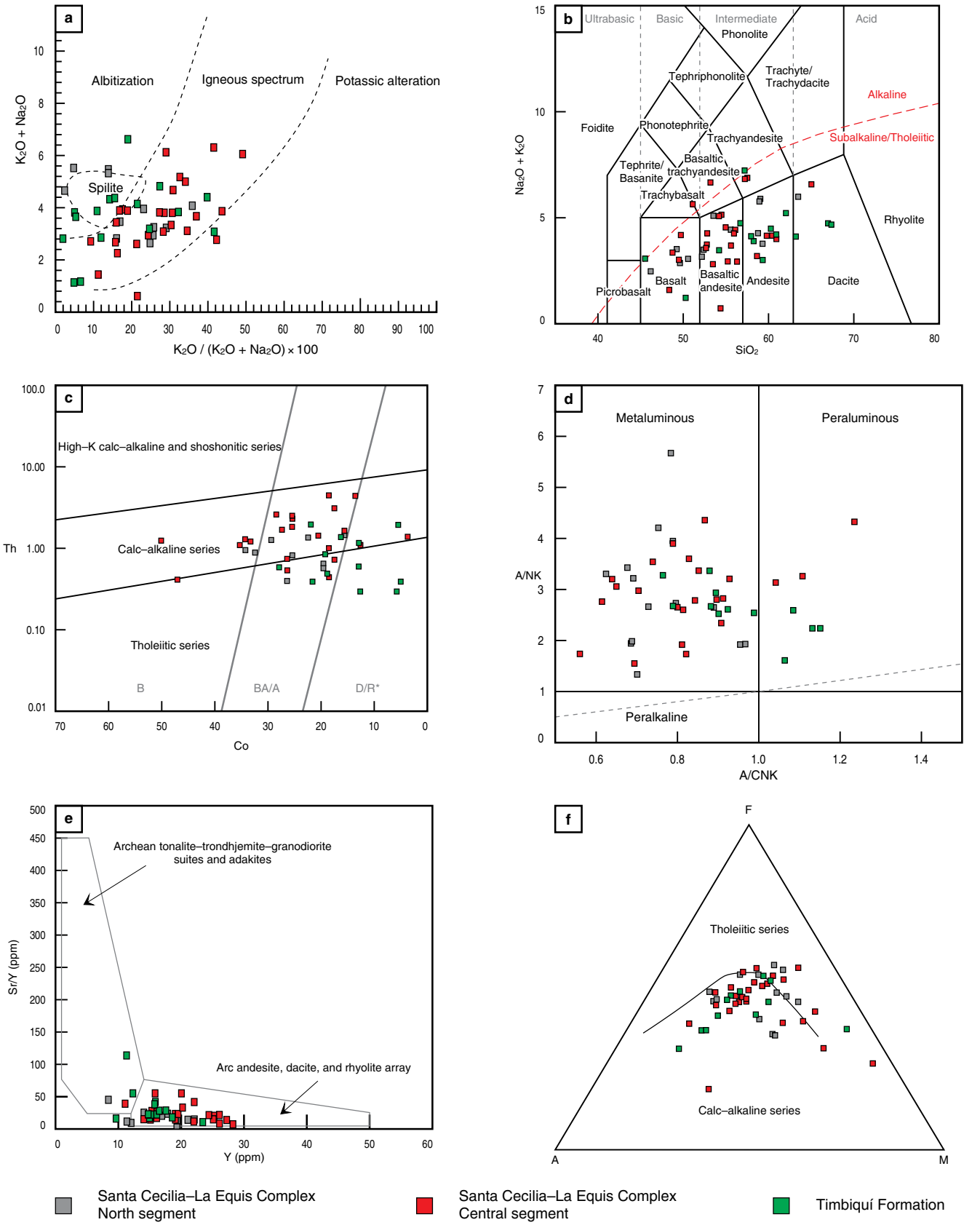

Figure 7. Classification and discrimination diagrams for the Santa Cecilia–La Equis Complex and the Timbiquí Formation vulcanites. **(a)** Hughes diagram (Hughes, 1972). **(b)** TAS diagram (Le Bas et al., 1986). **(c)** Co vs. Th diagram (Hastie et al., 2007). **(d)** Shand (1943) alumina saturation index diagram. **(e)** Y vs. Sr/Y diagram (Hansen et al., 2002). **(f)** AFM diagram (Irvine & Baragar, 1971). Santa Cecilia–La Equis Complex North segment (gray), Central segment (red), and Timbiquí Formation (green).

Table 1. Major oxides in rocks of the Santa Cecilia–La Equis Complex and Timbiquí Formation.

Sample	Latitude N	Longitude W	SiO_2	Al_2O_3	Fe_2O_3(T)	MnO	MgO	CaO	Na_2O	K_2O	TiO_2	P_2O_5	LOI	Total
Santa Cecilia–La Equis Complex (North segment)														
900009	8° 39' 51.42"	77° 21' 37.91"	55.34	14.87	8.34	0.14	2.94	7.23	2.95	0.56	0.68	0.13	5.06	98.24
900010	8° 39' 05.45"	77° 21' 52.11"	50.77	15.6	7.44	0.15	7.17	8.14	4.75	0.07	0.53	0.06	3.72	98.39
900081	8° 31' 45.04"	77° 17' 02.89"	62.93	12.91	9.05	0.14	2.64	4.78	5.72	0.25	0.71	0.08	0.61	99.83
900084	8° 34' 42.62"	77° 18' 28.11"	58.06	17.38	8.18	0.1	2.94	4.84	5.02	0.76	0.79	0.1	2.45	100.6
900087	8° 34' 34.97"	77° 20' 50.91"	47.63	19.86	9.59	0.15	4.13	11	2.44	0.96	0.74	0.17	2.75	99.44
900093	8° 31' 42.72"	77° 22' 23.07"	45.1	21.07	10.51	0.14	5.28	12.7	2.02	0.37	0.63	0.03	1.75	99.57
900296	8° 07' 31.37"	77° 07' 01.51"	50.37	16.18	9.37	0.17	5.73	10.1	2.52	0.83	0.62	0.14	3.57	99.6
900308	8° 06' 18.85"	77° 09' 39.201"	49.75	16.06	12.32	0.22	5.44	10.5	2.55	0.46	0.9	0.16	2.08	100.4
900315	8° 12' 17.71"	77° 07' 18.24"	57.45	16.83	7.67	0.12	3.54	6.87	3.26	0.93	0.61	0.28	3.06	100.6
900316	8° 12' 27.55"	77° 07' 15.13"	48	17.57	9.43	0.19	7.37	10.5	2.11	0.66	0.71	0.18	4.04	100.8
900317	8° 11' 57.56"	77° 07' 31.21"	54.39	16.72	7.15	0.12	5.15	9.15	2.83	1.51	0.48	0.16	3.01	100.7
Santa Cecilia–La Equis Complex (Central segment)														
7103	6° 39' 47.33"	76° 17' 24.50"	51.49	15.88	9.97	0.15	5.12	10.6	2.49	1.03	0.67	0.25	2.16	99.75
7106	6° 50' 31.77"	76° 21' 23.74"	55.63	18.16	7.29	0.1	2.8	6.71	3.56	1.75	0.65	0.25	3.17	100.1
95494	6° 05' 44.59"	76° 13' 37.71"	55.03	17.86	6.26	0.18	2.22	6.94	3.94	2.66	0.5	0.36	4.17	100.1
95498	6° 04' 57.70"	76° 14' 30.042"	50.3	17	7.59	0.26	3.65	7.7	2.91	1.23		0.8		99.85
95499	6° 05' 44.59"	76° 13' 37.71"	55.03	17.86	6.26	0.18	2.22	6.94	3.94	2.66		0.496	4.17	100.1
700567	6° 05' 47.68"	76° 29' 29.59"	51.74	18.18	9.3	0.1	4.61	9.19	2.18	0.56	0.68	0.11	2.97	99.62
119082	5° 29' 53.13"	76° 13' 55.029"	46.32	16.34	10.35	0.21	5.23	9.69	2.25	1.66	0.79	0.28	6.24	99.35
700717	6°26' 13.47"	76°34' 26.40"	55.02	18.2	8.9	0.16	3.41	10.1	2.68	0.25	0.64	0.17	1.08	100.6
700796	6° 12' 39.02"	76° 25' 55.40"	58.57	16.85	6.56	0.2	3.17	6.82	2.95	1.07	0.44	0.13	2.02	98.77
700812	6° 13' 32.43"	76° 28' 39.27"	54.96	14.24	7.52	0.15	7.43	9.77	2.43	0.43	0.47	0.13	1.16	98.7
700821	6° 21' 48.52"	76° 27' 44.11"	58.38	16.92	6.95	0.2	3.34	7.04	2.94	1.11	0.49	0.12	1.39	98.89
700830	6° 14' 46.76"	76° 29' 50.53"	57.77	17.1	8.06	0.11	2.79	8.7	2.41	0.73	0.46	0.12	1.11	99.36
700990	6° 05' 15.07"	76° 26' 40.26"	47.24	17.3	9.97	0.18	5.52	15.1	1.36	0.16	0.61	0.09	1.47	98.96
701803	5° 11' 15.55"	76° 16' 42.47"	50.47	20.1	7.41	0.13	3.78	8.41	3.39	0.66	0.74	0.28	5.09	100.5
702376	5° 04' 44.77"	76° 23' 48.88"	51.76	14.88	11.34	0.24	4.86	6.46	4.68	1.82	0.78	0.46	2.05	99.33
702476	5° 40' 38.55"	76° 25' 44.77"	47.47	11.24	11.54	0.19	11	10.7	1.71	1.19	0.61	0.28	2.77	98.69
702633	5° 14' 39.12"	76° 14' 12.20"	42.38	18.39	6.77	0.13	10.2	5.8	1.95	0.98	0.37			86.98

Table 1. Major oxides in rocks of the Santa Cecilia–La Equis Complex and Timbiquí Formation (*continued*).

Sample	Latitude N	Longitude W	SiO_2	Al_2O_3	Fe_2O_3(T)	MnO	MgO	CaO	Na_2O	K_2O	TiO_2	P_2O_5	LOI	Total
Santa Cecilia–La Equis Complex (Central segment)														
702760	5° 10' 53.08"	76° 12' 28.28"	59.89	15	7.42	0.14	3.8	7.16	2.52	1.41	0.52	0.19	2.36	100.4
702769	5° 10' 29.61"	76° 04' 46.64"	63.59	15.3	2.72	0.1	3.84	5.32	3.37	3.07	0.28			97.59
702999	6° 09' 12.56"	76° 15' 03.31"	47	15	3.52	0.28	7.96	11.19	0.5	0.13		0.85		99.47
703017	6° 05' 18.37"	76° 14' 05.75"	50.48	18.25	7.47	0.23	2.4	8.43	3.34	1.42		0.513	6.52	99.54
703084	6° 14' 30.17"	76° 20' 26.37"	54.52	20.21	7.84	0.15	2.9	7.07	3.47	0.7	0.52	0.11	2.64	100.1
706407	7° 00' 52.75"	76° 17' 53.74"	50.01	14.01	11.73	0.17	5.42	9.31	3.79	1.74	0.98	0.57	2.47	100.2
706413	6° 45' 40.43"	76° 17' 19.93"	46.85	16.11	12.2	0.18	6.76	9.46	1.91	1.3	1.06	0.22	3.82	99.88
Timbiquí Formation (South segment)														
APO–0036–P	2° 41' 07.47"	77° 09' 21.27"	58.14	18.73	3.33	0.11	1.54	6.34	3.62	1.3	0.35	0.19	6.2	99.81
APO–0054–LG	2° 44' 06.76"	77° 13' 58.16"	61.65	16.87	6.57	0.15	2.7	4.91	3.86	0.18	0.52	0.13	2.3	99.85
APO–0065–LT	2° 46' 52.80"	77° 14' 22.43"	54.39	17.44	7.91	0.19	3.22	7.25	2.81	1.77	0.55	0.25	4	99.79
APO–0069–LT	2° 47' 37.17"	77° 14' 57.76"	58.44	16.85	6.93	0.21	2.8	6.58	3.48	0.9	0.48	0.16	3	99.85
CDG–0254P	2° 03' 59.93"	77° 35' 39.85"	58.45	15.94	6.82	0.17	4.26	8.78	2.95	0.04	0.91	0.12	1.4	99.84
CDG–0256BP	2° 03' 59.93"	77° 35' 39.85"	49.17	16.56	7.18	0.13	9.64	13.45	1.13	0.05	0.45	0.04	1.9	99.77
CDG–0260P	2° 03' 55.80"	77° 33' 56.72"	57.59	16.91	6.75	0.12	4.4	8.3	3.73	0.18	0.77	0.13	0.9	99.84
CDG–0262P	2° 04' 17.98"	77° 33' 37.67"	54.76	16.95	7.64	0.12	3.22	7.2	2.71	1.23	0.43	0.19	5.3	99.71
CDG–0267P	2° 04' 44.40"	77° 32' 11.37"	54.88	17.33	8.7	0.15	3.97	3.02	5.7	1.26	0.62	0.27	3.8	99.7
CDG–0272P	2° 05' 32.02"	77° 31' 02.13"	52.31	17.11	10.2	0.2	4.6	7.88	2.56	0.8	0.67	0.2	3.2	99.76
CLM–0436	2° 25' 43.76"	77° 32' 11.34"	65.18	16.21	4.52	0.19	2.22	3.75	3.94	0.68	0.34	0.14	2.7	99.88
CLM–0454	2° 24' 35.22"	77° 29' 25.09"	59.64	17.08	6.9	0.2	2.83	6.54	3.71	0.42	0.45	0.14	1.9	99.85
CLM–0436–L	2° 25' 43.76"	77° 32' 11.34"	65.75	16.19	4.4	0.19	2.05	3.87	3.98	0.62	0.34	0.12	2.4	99.89

Source: Data from Buchely et al. (2009), Geología Regional y Prospección Ltd. (2014a, 2014b, 2014c), Rodríguez et al. (2010a, 2010b), and this research.

ducted plate, with light rare earth elements (LREE) enriched by 10–100 times and depletion ≤10 in heavy rare earth elements (HREE) (Figure 8).

The Eu/Eu* ratios are close to 1 for the Santa Cecilia–La Equis Complex and the Timbiquí Formation. $(La/Yb)_n$ ratios range between 1 and 5, with slightly higher values in the Central segment of the Santa Cecilia–La Equis Complex and slightly lower values for the Timbiquí Formation. The $(La/Sm)_n > 1$ ratio shows that LREE are increased relative to HREE in all samples.

4.4. Geochemistry of Intrusive Rocks

The Acandí Batholith presents SiO_2 values that range between 47.68% and 62.86% (sample 900328 shows a high value of 72.68%), low K_2O contents between 0.06 and 0.83%, TiO_2 <1%, MgO between 2.27 and 5.04% (sample 900008 shows a value of 10.16%), and CaO between 1.35 and 5.58%. The Mandé Batholith includes rocks with SiO_2 values between 44.30 and 70.91%, low K_2O contents between 0.06 and 1.69%, TiO_2 <1%, MgO between 1.20 and 8.05% (except samples RM–3508, 700784 with values of 11.1 and 14.2%), and CaO between 2.14 and 15.10%. The Napi Tonalite presents SiO_2 between 41.08 and 64.43%, low K_2O contents between 0.08 and 2.31%, TiO_2 <1%, MgO between 1.05 and 7.38%, and CaO between 4.55 and 14.07%. For the three plutons, the Al_2O_3, CaO, MgO, and TiO_2 contents decrease as SiO_2 increases. Na_2O increases with SiO_2, albeit with greater dispersion than other major elements (Table 2).

The chemical classification of the samples is very consistent with the petrographic classification of the Acandí and Mandé Batholiths and Napi Tonalite. These rocks vary in composition among gabbro, granodiorite, diorite, tonalite, peridotite–gabbro (Munchica Intrusive, samples MZD–0014 and CAQ–0416), and granite with high SiO_2 values (Acandí and Mandé Batholiths, samples 900328 and 174670, respectively) (Figure 9a, 9b).

Rocks are mostly basic to intermediate and metaluminous with A/CNK ratios between 0.6 and 1.1 and A/NK values between 1.5 and 5. A few samples are peraluminous (Figure 9c), probably due to sediment contamination, based on the low values for LOI (Table 2).

The rocks of the Acandí, Mandé, and Napi Intrusives are low–K tholeiitic to calc–alkaline. Several that are rich in MgO are grouped separately (RM–3508, 7111, 700784, and 900008). In these samples, the SiO_2 content is not a factor to separate the two series (Figure 9e).

In the alkali–lime index (MALI) and Fe–index diagrams (Frost et al., 2001; Frost & Frost, 2008), the rocks of the Acandí, Mandé, and Napi Intrusives are dominantly calcic granites with alkali–lime index values between –13.83 and 3.52. Additionally, these rocks plot in the field of magnesian granitoids, which are probably related to island arc magmas that followed relatively oxidizing differentiation trends (Figure 9d, 9f; Frost et al., 2001). The magnesian series show a close affinity to relatively hydrous, oxidizing magmas, and source regions (Frost & Lindsley, 1991), which is broadly consistent with subduction–related origins.

The Acandí and Mandé Batholiths and Napi Tonalite show similar patterns of trace elements vs. N–MORB, with negative Nb, Ti, and Zr anomalies and positive anomalies and high values of Cs, Ba, Th, Sr, and Rb. These are common features of magmas generated in an arc environment (Pearce, 1996; Pearce et al., 1984) in which a progressive decrease in LILE toward HFSE occurs (Figure 10). The Nb anomalies are similar for the three plutons (samples 700967, 700784, and 7135 of the Mandé Batholith show a positive Y anomaly).

The REE patterns normalized to the Nakamura chondrite (Nakamura, 1974) in the Acandí Batholith rocks show a negative slope. Two samples show a slightly flat pattern (900059 and 900304), and samples 900008 and 900311 are more depleted and primitive, with values that are 10 times less than the chondrite values in LREE and HREE (sample 900311 has a positive Eu anomaly). The REE patterns for all samples are similar to those of rocks generated in subduction environments above the subducted plate (Figure 10).

The Mandé Batholith rocks show parallel REE patterns, with few samples with flatter patterns that segment the main pattern (174670, 700967, and 700618). The most primitive rocks of the Mandé Batholith show REE values <10 times those of chondrites with positive Eu anomalies, and those with LREE values >10 show slight negative Eu anomalies. The REE patterns for all Mandé Batholith samples are similar to those of rocks generated in arcs, with a negative slope from LREE to HREE (Figure 10).

The Napi Tonalite presents several patterns. Some samples show patterns similar to oceanic crust rocks (CLM–0449P, CLM–0377P, CLM–388P, and APO0056LG), with decreasing LREE and flat HREE. The remaining samples show negative slopes from LREE to HREE, similar to patterns of rocks generated in arc environments. At least three different patterns are identified in these two plutons (Figure 10).

The Eu/Eu* ratios for the samples from the Acandí and Mandé Batholiths and the Napi Tonalite are between 0.71 and 1.45, many of which are near 1. Values of $(La/Yb)_n$ are between 1 and 5.5 (except for samples RM–3501, RM–3509, and 7105 of the Mandé Batholith with values of 14.5, 8.1, and 6.4, respectively) and $(La/Yb)_n < 1$ in some Napi Tonalite rocks (CLM–0447P, APO–0107–D, CAQ–0416–P, CLM–0377–P, and CLM–0388–P), with overall values of $(La/Yb)_n$ that are lower than those of the Acandí and Mandé Batholiths. The Mandé and Acandí Batholith ratios are $(La/Sm)_n > 1$ in all rocks, showing LREE enrichment relative to HREE. Napi Tonalite samples CLM–0447P, APO–0107D, CAQ–0416P, CLM–0388P, and MZD–0010–L have values of $(La/Sm)_n$

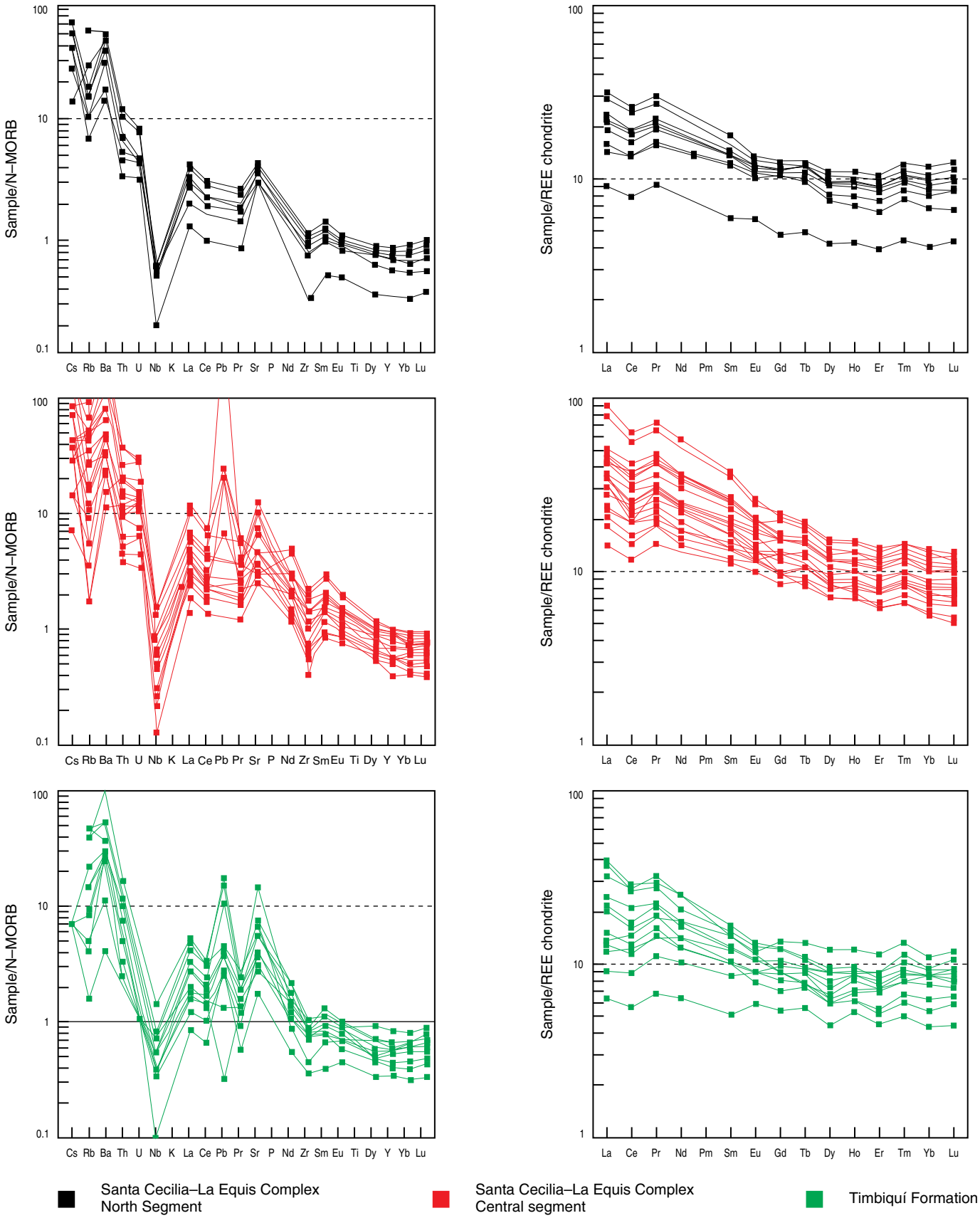

Figure 8. Multi–element diagrams normalized to N–MORB (Sun & McDonough, 1989) and rare earth element diagrams normalized to Nakamura chondrite (Nakamura, 1974) for volcanic rocks of the Chocó–Panamá Arc. Santa Cecilia–La Equis Complex North segment (black), Central segment (red), and Timbiquí Formation (green).

Table 2. Major oxides in rocks of the Acandí Batholith, Mandé Batholith, and Napi Tonalite.

Sample	Latitude N	Longitude W	SiO_2	Al_2O_3	Fe_2O_3(T)	MgO	CaO	Na_2O	K_2O	TiO_2	P_2O_5	MnO	LOI
Acandí Batholith													
900008	8° 35' 45.81"	77° 21' 25.99"	50.99	15.97	6.79	10.1	13.3	1.35	0.11	0.19	0.05	0.13	2.1
900059	8° 38' 15.66"	77° 23' 46.28"	56.64	14.88	9.98	4.86	6.02	4.98	0.06	0.83	0.12	0.16	2.42
900064	8° 35' 09.51"	77° 22' 57.50"	61.71	16.77	5.69	2.55	6.06	3.5	0.19	0.37	0.17	0.16	3.63
900072	8° 30' 30.33"	77° 20' 00.68"	61.14	16.42	6.67	2.69	6.76	3.02	0.96	0.46	0.14	0.16	0.6
900090	8° 31' 23.07"	77° 20' 40.94"	62.86	16.89	5.76	2.24	6.42	3.25	0.73	0.41	0.12	0.17	1.72
900304	8° 03' 20.04"	77° 07' 46.85"	49.41	20.27	9.9	4.84	11.2	2.17	0.54	0.75	0.27	0.19	1.33
900307	8° 06' 28.33"	77° 09' 08.31"	50.09	18.96	9.71	4.87	10.2	2.96	0.93	0.75	0.18	0.18	1.89
900311	8° 02' 23.15"	77° 06' 27.52"	47.68	21.12	9.97	5.04	13.2	1.59	0.35	0.7	0.04	0.16	0.96
900328	8° 02' 49.75"	77° 09' 49.48"	72.14	13.96	3.75	0.72	2.27	5.58	0.19	0.55	0.09	0.06	1.09
900369	8° 17' 10.70"	77° 10' 24.99"	62.39	16.22	6.27	2.96	6.26	2.98	0.77	0.48	0.09	0.14	1.19
900378	8° 07' 12.33"	77° 05' 59.81"	60.58	16.88	6.58	2.95	7.83	3.44	0.13	0.46	0.14	0.13	0.68
900059	8° 38' 15.66"	77° 23' 46.28"	56.64	14.88	9.98	4.86	6.02	4.98	0.06	0.83	0.12	0.16	2.42
900448	8° 12' 09.58"	77° 05' 57.73"	59.81	17.1	6.86	3.27	7.29	2.9	0.75	0.48	0.14	0.19	1.29
Mandé Batholith													
7072	6° 29' 06.85"	76° 28' 32.33"	58.38	18.3	7.03	3.07	8.12	3.16	0.56	0.47	0.16	0.17	1.08
7074	6° 25' 42.301"	76° 28' 41.52"	52.45	19.41	9.22	4.12	9.3	3.15	0.56	0.66	0.21	0.23	1.33
7075	6° 25' 27.51"	76° 28' 21.98"	64.81	16.25	5.19	2.26	5.42	3.59	1.12	0.43	0.13	0.12	0.72
7076	6° 25' 14.43"	76° 22' 53.54"	50.57	16.83	11.04	6.53	11.4	2.42	0.3	0.59	0.17	0.21	0.7
7110	6° 32' 11.04"	76° 27' 00.14"	63.26	14.43	7.67	3.04	6.08	2.97	1.4	0.72	0.23	0.12	0.74
7111	7° 06' 10.27"	76° 40' 28.23"	48.2	17.65	8.03	9.3	13.8	1	0.24	0.3	0.04	0.19	1.44
7134	6° 06' 04.45"	76° 16' 05.12"	61.82	16.02	6.6	2.39	5.19	4	1.93	0.59	0.22	0.14	0.67
7135	6° 07' 16.04"	76° 15' 56.88"	49.43	17.16	11.12	5.76	10.39	2.7	0.46	0.66	0.12	0.18	0.86
7146	6° 59' 17.26"	76° 35' 58.84"	68.6	15.72	3.66	1.58	4.71	3.2	1.15	0.31	0.12	0.11	1.22
7149	6° 57' 33.91"	76° 38' 48.34"	63.4	16.8	5.31	2.21	6.05	3.36	0.81	0.4	0.15	0.16	0.8
7195	5° 38' 45.78"	76° 19' 22.44"	54.09	17.37	9.13	4.08	8.04	3.11	1.2	0.78	0.25	0.16	1.48
80912	5° 10' 55.37"	76° 39' 19.06"	49.11	23.41	5.57	5.05	15.1	1.16	0.14	0.16	0.02	0.09	1.18
95177	7° 01' 17.51"	76° 38' 09.69"	48.76	17.9	11.91	6.17	12.2	1.25	0.23	0.72	0.01	0.19	0.87
95181	4° 36' 30.25"	76° 38' 36.56"	64.21	16.49	6.19	2.3	5.35	3.28	0.18	0.46	0.13	0.21	1.92
95765	7° 04' 47.96"	76° 35' 38.95"	63.69	16.64	5.4	2.3	5.68	3.47	1.36	0.41	0.13	0.14	1.1
95768	7° 02' 03.22"	76° 35' 03.28"	63.52	17.12	5.32	2.19	5.89	3.61	1.23	0.4	0.14	0.16	0.91

Table 2. Major oxides in rocks of the Acandí Batholith, Mandé Batholith, and Napi Tonalite (*continued*).

Sample	Latitude N	Longitude W	SiO_2	Al_2O_3	Fe_2O_3(T)	MgO	CaO	Na_2O	K_2O	TiO_2	P_2O_5	MnO	LOI
Mandé Batholith													
95774	5° 37' 43.35"	76° 35' 48.69"	62.53	16.93	5.88	2.21	6.07	3.4	1.19	0.44	0.15	0.16	0.78
95829	6° 51' 07.30"	76° 34' 56.14"	67.02	16.69	4.03	1.64	4.9	3.85	1.29	0.32	0.13	0.15	0.87
95830	7° 00' 43.88"	76° 34' 55.22"	65.16	16.38	4.97	2.02	5.65	3.44	1.22	0.37	0.14	0.15	1.35
95836	6° 41' 26.32"	76° 36' 03.16	63.39	16.98	5.66	2.39	6.25	3.42	1.13	0.42	0.15	0.17	0.66
174670	6° 43' 33.17"	76° 34' 22.09"	70.91	16.73	2.16	1.2	2.14	4.27	1.69	0.14	0.09	0.02	1.65
700130	5° 39' 08.28"	76° 19' 48.08"	54.11	18.03	8.17	3.78	8.09	3.43	1.12	0.63	0.21	0.18	2.52
700612	6° 12' 10.08"	76° 29' 44.23"	50.12	17.97	9.26	6.64	11.66	2.41	0.4	0.59	0.06	0.16	0.92
700615	6° 11' 14.65"	76° 28' 21.35"	53.77	17.77	8.67	4.98	9.51	2.84	0.31	0.67	0.13	0.15	1.01
700618	6° 12' 45.85"	76° 29' 08.41"	53.36	14.53	9.08	8.05	10.82	1.37	0.73	0.52	0.08	0.14	1.29
700784	6° 13' 55.21"	76° 20' 50.65"	47.76	10.39	11.17	14.2	10.47	1.27	0.32	0.39	0.06	0.23	2.58
700817	6° 20' 40.86"	76° 25' 44.52"	16.5	7.98	7.98	3.17	6.16	3.83	0.39	0.45	0.21	0.2	2.37
700852	6° 23' 03.83"	76° 22' 30.13"	50	15.78	11.73	7.58	8.57	3.07	0.37	0.58	0.19	0.18	1.98
700853	6° 20' 17.90"	76° 23' 26.08"	55.29	15.63	9.3	5.74	9.49	2.41	0.39	0.5	0.14	0.14	1.16
700854	6° 23' 56.04"	76° 24' 01.78"	54.39	15.52	9.71	5.25	8.93	2.81	0.87	0.87	0.31	0.16	1.19
700875	6° 33' 58.32"	76° 25' 12.59"	50.22	17.82	8.84	7.15	10.7	2.55	1.22	0.53	0.1	0.15	1.58
700905	6° 16' 46.15"	76° 21' 22.94"	44.3	20.5	12.09	6.35	13.48	1.03	0.06	0.56	0.02	0.17	0.51
700952	5° 10' 48.67"	75° 09' 33.70"	54.56	20.19	5.94	3.4	10.5	3.01	0.28	0.36	0.13	0.06	1.33
700967	6° 24' 15.02"	76° 19' 44.70"	47.77	19.06	11.02	5.77	10.07	2.9	0.5	0.72	0.15	0.27	1.31
700972	6° 09' 36.36"	76° 19' 55.71"	47.83	18.96	10.5	4.83	10.32	3.06	0.38	0.75	0.27	0.21	1.51
700977	6° 07' 52.42"	76° 22' 43.35"	49.64	18.12	10.97	6.17	11.23	2.21	0.15	0.59	0.1	0.18	0.71
701005	6° 07' 09.47"	76° 15' 16.24"	52.43	17.58	8.87	5.14	7.97	2.87	1.21	0.53	0.15	8.87	2.89
701012	6° 06' 40.26"	76° 16' 13.20"	65.78	15.6	4.83	2.22	5.01	3.63	1.58	0.39	0.16	–0.5	0.89
701153	6° 11' 08.03"	76° 26' 42.15"	62.53	16.71	4.8	3.12	6.9	3.49	0.57	0.46	0.11	0.18	1.1
701155	6° 11' 44.047"	76° 29' 47.51"	48.2	18.32	9.04	8	12.92	1.39	0.11	0.38	0.02	0.16	1.13
701728	6° 42' 05.88"	76° 18' 54.27"	55.98	17.77	8.53	4.08	7.18	3.28	1.14	0.58	0.16	0.12	1.53
GZ–1818	7° 00' 10.79"	76° 28' 35.70"	58.33	16.09	7.87	4.37	8.79	2.74	0.52	0.5	0.11	0.14	1.11
GZ–1867	5° 39' 05.97"	76° 28' 41.31"	58.79	14.6	8.17	4.6	5.99	4.28	0.7	0.88	0.08	0.14	1.65
HCA–1208	6° 46' 48.58"	76° 30' 55.11"	54.2	14.17	10.57	6.62	9.28	2.12	1.19	0.63	0.14	0.2	0.86
HCA–1215	6° 39' 50.28"	76° 30' 45.82"	50.57	16.17	9.72	7.88	11.3	2.51	0.38	0.51	0.12	0.18	1.24
HCA–1221	6° 41' 14.89"	76° 30' 19.68"	54.11	17.25	8.8	5.19	9.88	2.81	0.69	0.51	0.13	0.17	1.13

Table 2. Major oxides in rocks of the Acandí Batholith, Mandé Batholith, and Napi Tonalite (*continued*).

Sample	Latitude N	Longitude W	SiO_2	Al_2O_3	$Fe_2O_3(T)$	MgO	CaO	Na_2O	K_2O	TiO_2	P_2O_5	MnO	LOI
Mandé Batholith													
HCA–1278	6° 41' 22.42"	76° 26' 30.14"	56.93	18.22	6.97	2.75	8.44	3.31	1.12	0.45	0.28	0.14	2.38
HCP–1437	6° 42' 11.33"	76° 29' 51.94"	61.04	15.16	7.61	2.86	6.54	3.52	1.28	0.62	0.17	0.15	0.75
RM–3501	6° 49' 02.03"	76° 30' 48.44"	51.65	17.62	10.04	4.49	8.21	3.41	0.52	0.66	0.18	0.16	1.54
RM–3508	6° 48' 34.40"	76° 31' 19.41"	50.96	10.85	8.11	11.1	12.9	1.25	1.45	0.47	0.26	0.16	2.1
RM–3509	6° 52' 49.91"	76° 31' 07.71"	59.48	15.42	7.9	3.27	7.35	2.85	1.66	0.66	0.21	0.15	0.82
RM–3518	6° 53' 43.63"	76° 31' 10.91"	56.46	16.07	8.09	4.61	8.37	2.86	1.4	0.59	0.26	0.13	1.34
RM–3520	5° 12' 15.75"	76° 31' 33.38"	49.78	18.43	9.7	5.96	10	3.45	0.41	0.49	0.07	0.17	1.75
RM–3529	6° 50' 05.41"	76° 29' 30.20"	49	18.34	10.11	5.77	12.3	2.31	0.27	0.58	0.11	0.14	0.87
RM–3539	5° 11' 36.02"	76° 31' 17.17"	55.62	17.74	7.91	4.56	8.44	3.01	0.52	0.51	0.11	0.13	1.9
RM–3548	5° 10' 02.24"	76° 30' 52.90"	67.57	14.7	4.96	1.82	4.86	4.65	0.29	0.54	0.16	0.07	0.88
Napi Tonalite													
APO–0049	2° 43' 17.35"	77° 12' 37.93"	60.64	17.55	5.95	2.93	5.77	3.52	0.92	0.47	0.15	0.15	1.8
APO–0056	2° 44' 32.22"	77° 14' 26.14"	55.47	17.67	7.81	4.26	8.72	3.04	0.11	0.6	0.09	0.15	1.9
APO–0107–D	2° 38' 47.74"	77° 20' 33.98"	56.93	17.65	7.79	3.39	8.07	2.96	0.23	0.52	0.13	0.17	2
CAQ–0190P	2° 52' 12.96"	77° 08' 36.50"	58.51	16.35	5.57	3.33	4.55	4.08	0.66	0.4	0.08	0.14	6.2
CAQ–0346–P	2° 23' 40.15"	77° 35' 07.08"	46.34	15.69	8.28	7.38	7.28	1.03	1.28	0.56	0.05	0.06	11.8
CAQ–0416–P	2° 09' 43.59"	77° 28' 05.96"	42.9	18.69	13.04	5.96	12.99	1.97	0.78	0.84	0.56	0.21	1.7
CAQ–0420R	2° 10' 36.14"	77° 27' 58.89"	56.75	16.65	6.45	3.96	7.33	4.14	1.02	0.59	0.25	0.13	2.5
CLM–0377–P	2° 30' 22.56"	77° 25' 17.53"	53.19	17.7	9.03	5.14	7.61	2.28	0.08	0.66	0.09	0.27	3.8
CLM–0388–P	2° 30' 33.65"	77° 27' 48.38"	52.94	19.96	4.68	5.15	8.32	4.8	0.45	0.66	0.12	0.1	2.6
CLM–0447–L	2° 24' 48.80"	77° 30' 38.43"	52.78	18.09	8.72	4.98	9.13	2.98	0.36	0.7	0.12	0.16	1.8
CLM–0447P	2° 24' 48.80"	77° 30' 38.43"	52.83	18.13	8.37	4.81	9.06	3	0.37	0.66	0.11	0.16	2.3
CLM–0449P	2° 24' 50.76"	77° 30' 18.24"	44.2	19.34	10.6	5.56	10.7	2.1	0.65	0.96	0.05	0.18	5.4
MZD–0010–L	2° 28' 21.36"	77° 20' 12.84"	53.09	18.95	7.93	2.94	8.48	3.46	2.31	0.58	0.43	0.21	1.3
MZD–0014–R	2° 28' 46.81"	77° 21' 08.27"	41.08	18.79	14.08	6.13	14.07	1.38	0.73	0.98	0.89	0.24	1.3
MZD–0022–R	2° 28' 28.85"	77° 22' 50.19"	64.43	16.79	3.64	1.05	4.99	4.12	1.43	0.28	0.13	0.08	2.9

Source: Data from Buchely et al. (2009), Geología Regional y Prospección Ltd. (2014a, 2014b, 2014c), Rodríguez et al. (2010a, 2010b), and this research.

< 1 with LREE decreasing relative to HREE, matching the REE pattern of the Nakamura chondrite (Nakamura, 1974) (Figure 10).

4.5. Geotectonic Environment of the Chocó–Panamá Arc

The geochemical discrimination and tectonic environment diagram of Condie & Kröner (2013) shows similar distributions between the Santa Cecilia–La Equis Complex, Timbiquí Formation, the Acandí and Mandé Batholiths, and Napi Tonalite (Figure 11a, 11b). The volcanic and plutonic units of the Chocó–Panamá Arc plot in the field of continental arcs at the interface with oceanic arcs. In Pearce (2008) and Wood (1980) the samples are distributed within the active continental margin arc field with a few samples in the island arc field.

4.6. Geochronology

This study reports four new Ar–Ar ages: One from the Santa Cecilia–La Equis Complex, one from the Acandí Batholith, one from the Mandé Batholith and one from the porphyritic units that intrude the Acandí Batholith (Table 3).

Sample IGM–900317 is a porphyritic basalt of the Santa Cecilia–La Equis Complex collected in the Cutí River Basin, composed of plagioclase, clinopyroxene, and orthopyroxene phenocrysts in a microlitic matrix. The sample yields a three–stage plateau age of 45.3 ± 1.6 Ma, featuring 75.9% ^{39}Ar. The integrated age of sample IGM–900317 is 45.6 ± 1.6 Ma (Figure 12). The inverse isochron shows a linear trend, suggesting an age of 45.3 ± 2.6 Ma with MSWD = 0.64. The age was extracted from a whole–rock analysis and corresponds to the Lutetian Stage of the Eocene.

Few dates are available for the Santa Cecilia–La Equis Complex. Buchely et al. (2009) obtained an Ar–Ar age of 50.7 ± 2.0 Ma from a volcanic basalt glass, revealing a plateau age of 55 Ma, interpreted as the total fusion age.

The tonalite sample IGM–900369 was collected from the Acandí Batholith along the Tanela River. It is an inequigranular, hypidiomorphic, fine– to medium–grained rock with plagioclase (51%), quartz, hornblende, and biotite. It presents a four–stage plateau with 62.5% ^{39}Ar, suggesting an age of 51.84 ± 2.14 Ma, and an integrated age of 51.54 ± 2.04 Ma. The inverse isochron diagram reveals a linear trend in all points except at 900 °C, yielding an age of 48.13 ± 5.76 Ma with MSWD = 0.34 (Figure 13). The ages are from whole–rock analysis and correspond to the Ypresian Stage of the Eocene.

The Ar–Ar dating of tonalite from the Acandí Batholith agrees with the results of Buchely et al. (2009), yielding an age of 51.84 ± 2.14 Ma for this unit. Montes et al. (2015) published three U–Pb crystallization ages in zircon between 49.5 ± 0.9 and 49.7 ± 1.6 Ma. This range matches the age of the Mandé Batholith (Table 4).

The tonalite sample (IGM–706477) from the Mandé Batholith, collected along the Medellín–Quibdó road between Carmen de Atrato and El Doce, yields an age range with three high–temperature stages. A plateau featuring 92.9% ^{39}Ar reveals an age of 53.07 ± 1.92 Ma, with an integrated age of 54.47 ± 2.1 Ma. The inverse isochron reveals a linear trend with an age of 49.49 ± 3.66 Ma, with MSWD = 0.29 (Figure 14). Ages were extracted from hornblende and correspond to the Ypresian Stage of the Eocene.

The andesite porphyry sample IGM–900005 from the unit of andesitic porphyry bodies consists of plagioclase, hornblende, and biotite phenocrysts embedded in a felsite microcrystalline matrix. The sample yields a six–stage plateau with an age of 48.1 ± 2.0 Ma and an integrated age of 47.1 ± 2.0 Ma (86.3% ^{39}Ar). The inverse isochron shows a linear trend yielding an age of 46.2 ± 5.4 Ma, with MSWD = 1.6 (Figure 15). The age obtained from the whole–rock analysis corresponds to the Ypresian Stage of the Eocene.

5. Discussion and Conclusions

5.1. Arc Composition

The Chocó–Panamá Arc in Colombia is exposed against the western margin of the Colombia Plateau and is fragmented in segments extending from Panamá to Ecuador. At least three segments or blocks are similar in lithology, geochemical composition, and age. Previous research has associated the Timbiquí Formation and the Napi Tonalite with the Santa Cecilia–La Equis Complex and the Mandé Batholith (Echeverri et al., 2015; Geología Regional y Prospección Ltd., 2014a, 2014b, 2014c; Rodríguez et al., 2010a), although this correlation remained unsupported. Additionally, the San Blas Complex and the Azuero Marginal Complex in Panamá have been associated with the Chocó–Panamá Arc (Barat et al., 2014; Montes et al., 2012; Ramírez et al., 2016).

The Chocó–Panamá Arc is formed of volcanic units (Santa Cecilia–La Equis Complex, Timbiquí Formation) composed of basalt, andesite, and dacite lava flows, pillow lavas, and pyroclastic rocks such as breccias, agglomerates, and tuffs (Buchely et al., 2009; Calle & Salinas, 1986; Cossio, 1994; Geología Regional y Prospección Ltd., 2014a, 2014b, 2014c; González, 2001; Rodríguez et al., 2010b, 2013) and plutonic units (Mandé, Acandí Batholiths and Napí Tonalite), of gabbroic to granitic composition, with prevailing quartz diorite and tonalite.

The petrographic and geochemical data suggest that the initial composition of the arc was metaluminous subalkaline tholeiitic basaltic lavas and gabbros that later evolved to calc–alkaline continental margin arc rocks, characterized by metalu-

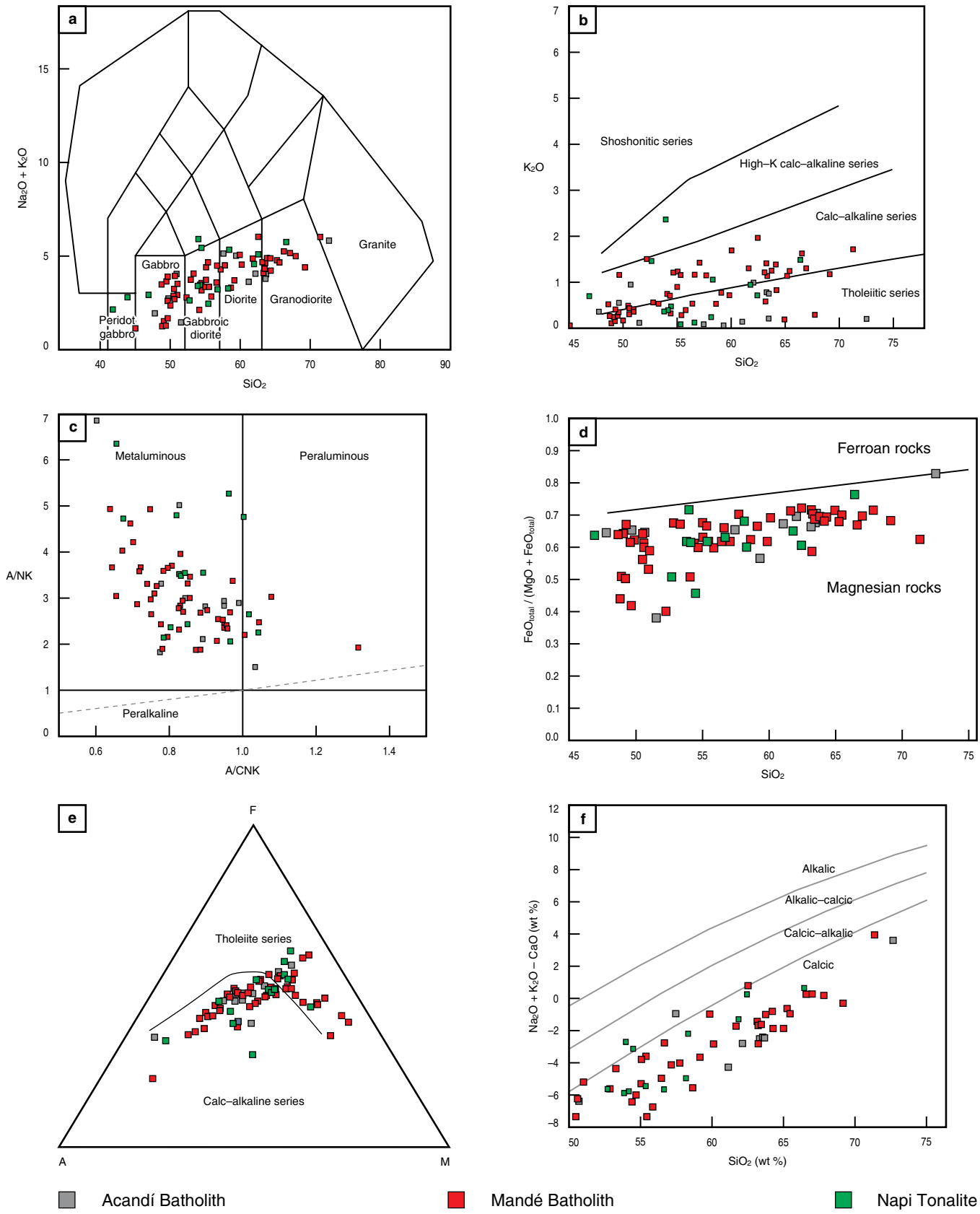

Figure 9. Classification diagrams for the Acandí Batholith (gray), Mandé Batholith (red), and Napi Tonalite (green). **(a)** TAS diagram (Middlemost, 1994). **(b)** K_2O vs. SiO_2 diagram (Peccerillo & Taylor, 1976). **(c)** Aluminosity–alkalinity diagram (Shand, 1943). **(d)** Diagram to discriminate between ferroan and magnesian rocks (Frost & Frost, 2008). **(e)** AFM diagram (Irvine & Baragar, 1971). **(f)** Alkali–lime vs. SiO_2 diagram after Frost et al. (2001).

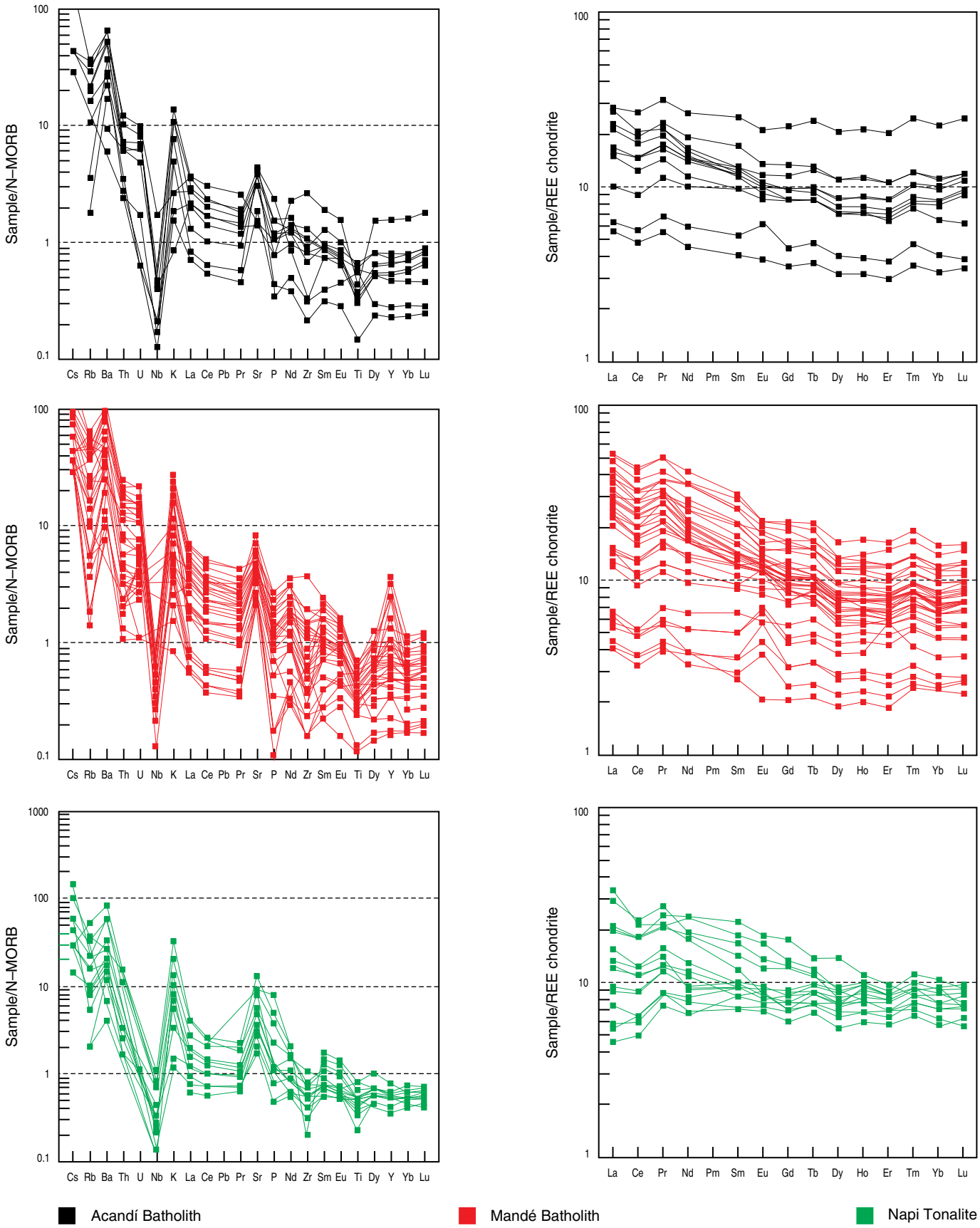

Figure 10. Trace elements vs. N–MORB diagram (Sun & McDonough, 1989) and rare earth elements vs. chondrite (Nakamura, 1974). Acandí Batholith (black), Mandé Batholith (red), and Napi Tonalite (green).

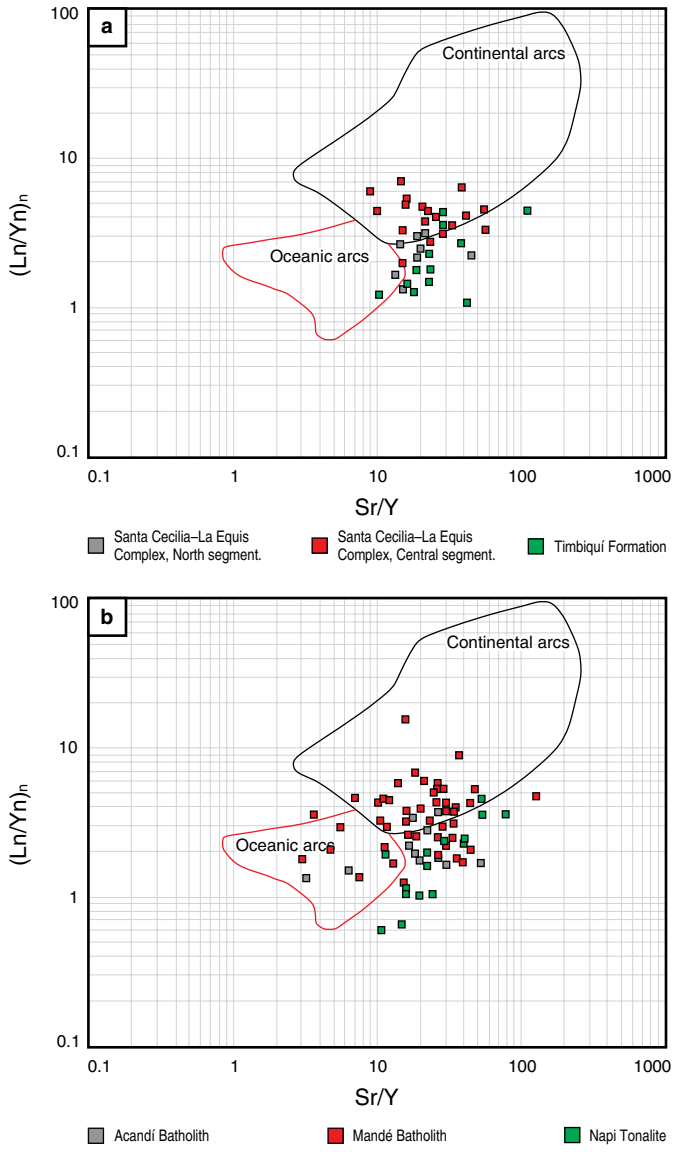

Figure 11. Tectonic environment discrimination diagrams for the Chocó–Panamá Arc (Condie & Kröner, 2013). **(a)** Santa Cecilia–La Equis Complex North segment (gray), Central segment (red), and Timbiquí Formation South segment (green). **(b)** Acandí Batholith (gray), Mandé Batholith (red), and Napi Tonalite (green).

minous subalkaline intermediate andesite and plutonic quartz diorites and tonalities, as sediments and water entered the mantle along the subducted slab (Álvarez & Parra, 1979; Guarín & Álvarez, 1975; Ingeominas & Organización de las Naciones Unidas, 1982; Ramírez et al., 1979; Sillitoe et al., 1982).

The multielement diagrams show that the igneous rocks studied have typical arc geochemical affinities. Trace element patterns are characterized by negative Nb, Ti, and Zr anomalies and positive Cs, Ba, Th, Sr, and Rb anomalies and depletions in LREE relative to HREE. Different REE patterns vs. chondrites are recognized in this research for both volcanic and plutonic

Table 3. Ar–Ar ages of rocks from the Chocó–Panamá Arc.

IGM	Latitude N	Longitude W	IIA (Ma) ± 2s	TFA (Ma) ± 2s	WMPA (Ma) ± 2s	Ca/K	Comments	Petrographic Observations
900317	8° 11' 57.5644"	77° 07' 31.2052"	45.3 ± 2.6	45.6 ± 1.6	45.3 ± 1.6	2.7–78.9	Three steps plateau	Porphyritic basalt Santa Cecilia– La Equis Complex
900369	8° 17' 10.7021"	77° 10' 24.9930"	48.13 ± 5.76	51.54 ± 2.04	51.84 ± 2.14	7.25–13.92	Four steps plateau	Acandí Batholith tonalite
706477	5° 44' 43.6155"	76° 16' 30.8074"	49.49 ± 3.66	54.47 ± 2.1	53.07 ± 1.92	2.31–24.98	Three steps high temperature plateau	Mandé Batholith tonalite
900005	8° 36' 53.0117"	77° 21' 44.3220"	46.2 ± 5.4	47.1 ± 2.0	48.1 ± 2.0	2.61–17.45	Six steps plateau	Porphyritic andesite–andesite and dacite

Note: (TFA) Total fusion age; (IIA) Inverse isochrone age; (WMPA) Weighted mean plateau age; (Ca/K) Apparent Ca/K ratios; (WMIPA) Weighted mean intermediate plateau age.

2s ± 1 = Estimated uncertainty (2s)

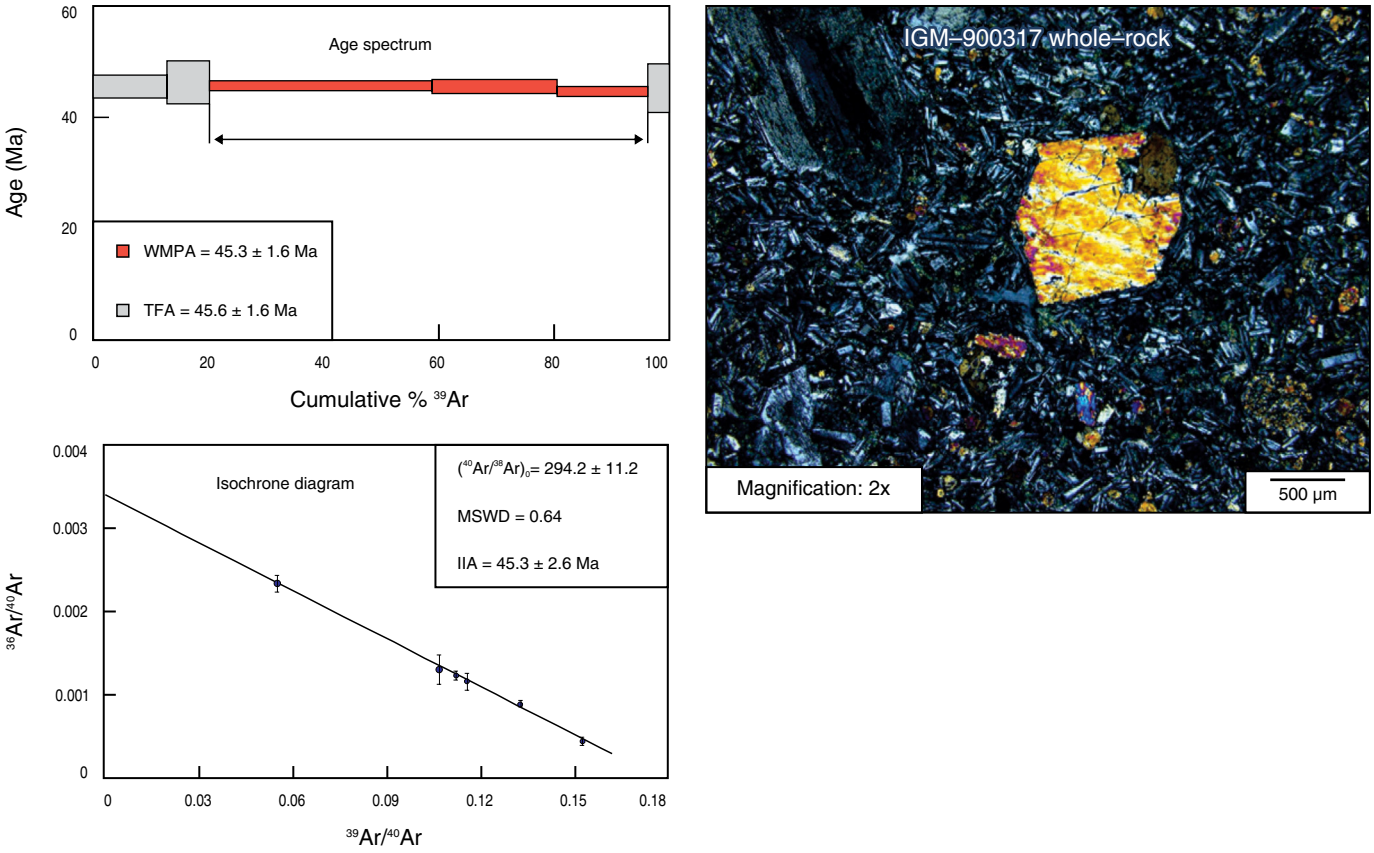

Figure 12. Sample IGM–900317 age range, Santa Cecilia–La Equis Complex basalt.

rocks, suggesting more than one magmatic pulse in the evolution of the Chocó–Panamá Arc.

5.2. Age

The ages of the different Chocó–Panamá Arc components (volcanic and plutonic rocks) are compiled in Gómez et al. (2015b) as a part of the Geological Map of Colombia (Table 4). The arc volcanic rocks from the Santa Cecilia–La Equis Complex (Central segment) yield Ar–Ar ages in volcanic glass of 50.7 ± 2.0 Ma, 55.1 ± 1.5 Ma, and 36.7 ± 11.5 Ma (Buchely et al., 2009). The latter age, with high error, suggests Ar loss and low reliability for the date. Such ages are considered close to the rock crystallization age because they were obtained in volcanic glass that cooled rapidly. In the Acandí zone (North segment), the Santa Cecilia–La Equis Complex yields a whole–rock Ar–Ar age of 45.3 ± 1.6 Ma (this study). For the Timbiquí Formation (South segment), McCourt et al. (1990) reported K–Ar ages of 53.4 ± 3 Ma and 41 ± 1 Ma (Ypresian – Bartonian) in andesites and 46.7 ± 2 Ma (Lutetian) for andesitic dikes that cut the unit, describing a pyroclastic event at 32.1 ± 3.5 Ma (Rupelian Stage of the Oligocene). These data suggest that volcanism in the Chocó–Panamá Arc occurred at least between 56.5 and 45 Ma (Ypresian – Lutetian).

The Acandí Batholith (North segment) yields a whole–rock Ar–Ar cooling age (tonalite) of 51.84 ± 2.14 Ma (this study). The Mandé Batholith (Central segment) presents a K–Ar date of 54.7 ± 1.3 (Sillitoe et al., 1982) to 34 Ma (Botero, 1975); Ar–Ar ages in basic facies (gabbronorite) between 53.6 ± 2.9 and 52.7 ± 3.2 Ma (Buchely et al., 2009), interpreted as closure ages of the pluton basic facies; and Ar–Ar ages in hornblende and biotite from the intermediate facies (tonalite) between 52.7 ± 3.2 and 48.0 ± 1.5 Ma (Buchely et al., 2009; this study), which correspond to cooling ages. Most of the Ar–Ar ages in tonalites are slightly younger than those of the basic facies, matching the macroscopic observations of the lithological relationships in the pluton (Table 4).

The Ar–Ar ages reported in this study are older than the zircon U–Pb ages obtained by Montes et al. (2015) 43.8 ± 0.8 Ma and 42.5 ± 1.3 Ma for the Mandé Batholith and ages between 49.7 ± 1.6 and 49.5 ± 0.9 Ma for the Acandí Batholith (Table 4). This discrepancy may be caused by excess argon or by analyses conducted in different facies of the pluton.

McCourt et al. (1990) determined K–Ar ages between 53 ± 5 and 39 ± 2 Ma (Ypresian – Bartonian) for the Napi Tonalite (South segment). Additionally, the authors suggest that the Balsitas Leucotonalite, with a K–Ar age of 48 ± 1 Ma (Ypresian), and an andesite dike that segments the leucotonalite, with an

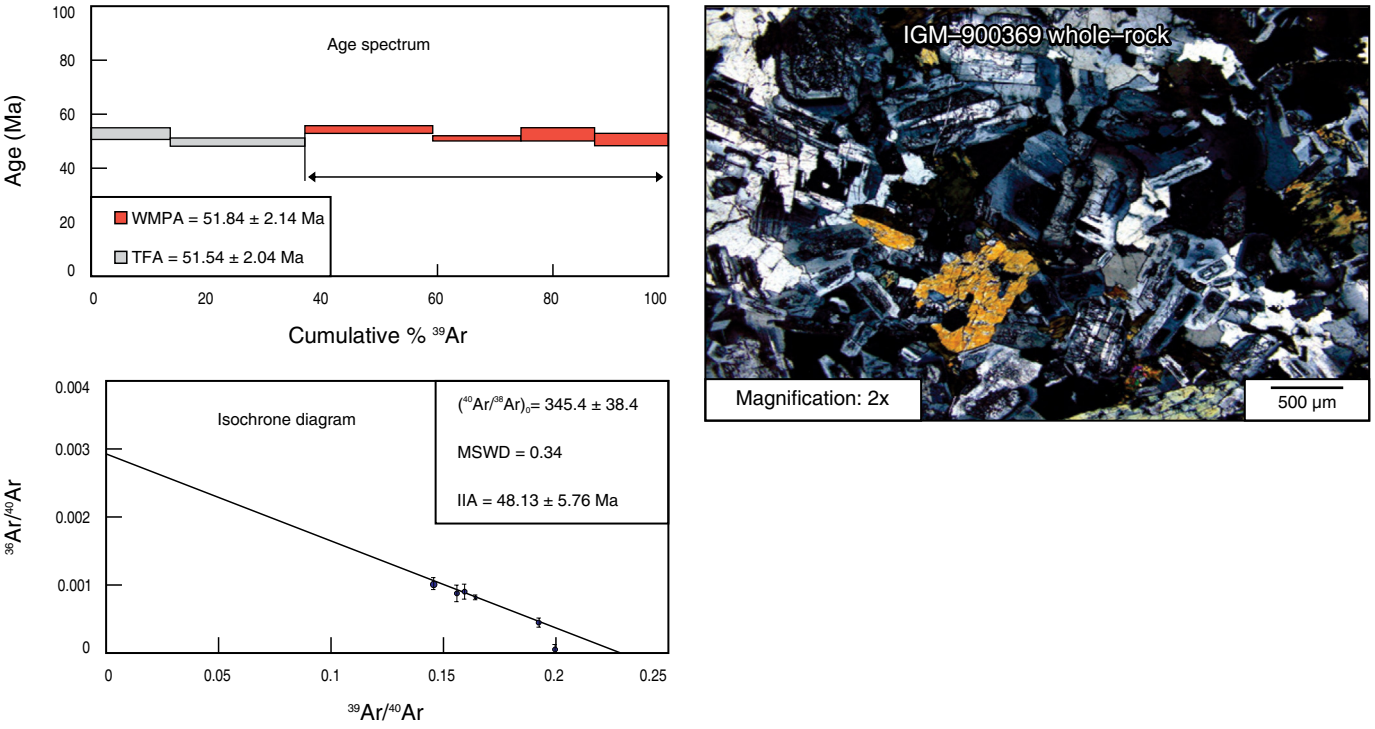

Figure 13. Sample IGM-900369 age range, Acandí Batholith tonalite.

age of 42.6 ± 1.3 Ma (Lutetian), are of similar lithological composition. El Salto Tonalite yields a K–Ar age of 51 ± 1 Ma (Ypresian) and is also correlated with the Napi Tonalite according to the authors (Table 4).

Geología Regional y Prospección Ltd. (2014a, 2014b, 2014c) report two U–Pb zircon LA–ICP–MS ages of 46.8 ± 0.7 Ma and 45.6 ± 0.6 Ma (Lutetian) for dioritic and granodioritic rocks associated with the Guapi Ultramafite.

Mineralized porphyry units intruding the volcanic rocks of the Santa Cecilia–La Equis Complex and the Acandí and Mandé Batholiths yield K–Ar and Ar–Ar cooling ages (Table 4) between 54.7 ± 1.3 (Murindó project) and 42.7 ± 0.9 Ma (Pantanos project) (Sillitoe et al., 1982). Leal-Mejía (2011) report two U–Pb zircon ages from mineralized porphyry units from the central sector, yielding crystallization ages of 45.3 ± 1.2 Ma and 44.6 ± 0.9 Ma. The K–Ar and Ar–Ar ages are considered minimum ages of the emplacement of the copper porphyry system and match those of Río Pito, an extension of the Acandí Batholith in Panamá (Sillitoe et al., 1982).

The K–Ar, Ar–Ar, and U–Pb ages of the plutonic rocks from the Acandí and Mandé Batholiths, Napi Tonalite, Balsitas Leucotonalite, El Salto Tonalite, dioritic and granodioritic facies associated with the Guapi Ultramafite, and units of mineralized andesitic and dacitic porphyries from the North and Central segments of the arc suggest that plutonism associated with the Chocó–Panamá Arc began ca. 56 Ma (Ypresian) and ended ca. 37 Ma (Bartonian). These ages are similar to the zircon U–Pb and Ar–Ar ages obtained in the San Blas and Azuero marginal complexes in Panamá (Montes et al., 2012; Ramírez et al., 2016; Wegner et al., 2011).

Wegner et al. (2011) report Ar–Ar ages in hornblende of 49.4 ± 1.0 Ma in the Cerro Azul Gabbro and 47.2 ± 1.3 Ma in the Mamoni Quartz diorite. Additionally, Montes et al. (2012), Ramírez et al. (2016), and Villagómez (2010) report that the cooling ages of the Mandé Batholith are similar to those of the San Blas Complex in Panamá and suggest that these plutonic bodies cooled and were exhumed during different episodes between 47 and 9 Ma by tectonic, volcanic, and erosional events.

The geochronological, stratigraphic, and lithogeochemical relationships of the Timbiquí Formation and Napi Tonalite present characteristics similar to those of the Acandí and Mandé Batholiths and the Santa Cecilia–La Equis Complex, suggesting that they are part of the Chocó–Panamá Arc and represent a dispersed segment of the arc.

5.3. Arc Basement

Buchs et al. (2010) and Montes et al. (2012) provide clear evidence of the occurrence of an oceanic plateau at the base of the Eocene volcanic arc in Panamá; however, little is known about the basement of the Chocó–Panamá Arc in Colombia. At the western edge of the North segment, the discordant marine sedimentites and breccia sequences of the Tripogadí Sedimentites and the Triganá Breccias (Rodríguez & Sierra, 2010; Rodríguez et al., 2010b) rest on an unknown basement. In the Central segment, the western boundary with the San José de

Table 4. Radiometric ages of different Chocó–Panamá Arc units (updated from Gómez et al., 2015b and Geología Regional y Prospección Ltd., 2014a, 2014b, 2014c).

Sample	Lithology	Latitude N	Longitude W	Age (Ma)	Dating method	Material analyzed	Reference
Santa Cecilia–La Equis Complex (North segment)							
IGM–900317	Porphyritic basalt	8° 11' 57.5644"	77° 07' 31.2052"	45.3 ± 1.6	Ar–Ar	Volcanic glass	Present study
Santa Cecilia–La Equis Complex (Central segment)							
IGM–706917	Porphyritic basalt	6° 44' 37.27"	76° 23' 20.65"	50.7 ± 2.0	Ar–Ar	Volcanic glass	Buchely et al. (2009)
Timbiquí Formation							
AM2589	Andesitic tuff	2° 17' 28.05"	77° 38' 45.82"	32.1 ± 3.5	K–Ar		McCourt et al. (1990)
HV309		2° 17' 31.77"	77° 09' 04.59"	33 ± 2	K–Ar		McCourt et al. (1990)
AM2588	Andesite	2° 17' 31.97"	77° 38' 54.48"	38.9 ± 4.3	K–Ar		McCourt et al. (1990)
BX12	Andesite	2° 23' 42.98"	77° 34' 29.58"	41.7 ± 1.2	K–Ar		McCourt et al. (1990)
BX70	Andesite	2° 12' 16.60"	77° 40' 39.02"	41 ± 1	K–Ar		McCourt et al. (1990)
BX72A	Andesite	2° 11' 01.67"	77° 42' 03.70"	44 ± 1	K–Ar		McCourt et al. (1990)
BX76	Timbiquí Formation dike	2° 10' 34.91"	77° 41' 56.95"	46.7 ± 2	K–Ar		McCourt et al. (1990)
BX72	Andesite	2° 11' 00.63"	77° 42' 13.12"	50.7 ± 2	K–Ar		McCourt et al. (1990)
BX71	Andesite	2° 11' 15.25"	77° 42' 20.19"	53.4 ± 3	K–Ar		McCourt et al. (1990)
Acandí Batholith							
IGM–900369	Tonalite	8° 17' 10.7021"	77° 10' 24.9930"	51.84 ± 2.14	Ar–Ar	Total rock	Present study
GA–001	Granitoide	8° 30' 33.84"	77° 20' 13.56"	49.5 ± 0.9	U–Pb	Zircon	Montes et al. (2015)
VM–001	Granitoide	8° 26' 21.48"	77° 19' 19.56"	49.7 ± 1.6	U–Pb	Zircon	Montes et al. (2015)
VM–003	Granitoide	8° 50' 54.492"	77° 20' 24.719"	49.5 ± 1.1	U–Pb LA–ICP–MS	Zircon	Montes et al. (2015)
Mandé Batholith							
Ch–51	Granodiorite	5° 43' 08.99"	76° 20' 56.17"	34	K–Ar	Biotite	Botero (1975)
IGM–304958	Quartzodiorite	8° 32' 03.45"	77° 25' 01.08"	38.9 ± 3	K–Ar	Sericite	Álvarez & Parra (1979)
IGM–706956	Tonalite	6° 48' 31.90"	76° 35' 26.53"	48.0 ± 1.5	Ar–Ar	Hornblende and biotite	Buchely et al. (2009)
UAKA 80–22	Tonalite	8° 27' 51.45"	77° 49' 01.18"	48.1 ± 1	K–Ar	Hydrothermal sericite	Sillitoe et al. (1982)
IGM–706477	Tonalite	5° 44' 43.6155"	76° 16' 30.8074"	53.07 ± 1.92	Ar–Ar	Total rock	Present study
IGM–706957	Tonalite	6° 48' 31.90"	76° 35' 26.53"	48 ± 1.5	Ar–Ar	Hornblende and biotite	Buchely et al. (2009)
IGM–707151	Gabbronorite	6° 34' 0.50"	76° 35' 29.06"	52.7 ± 3.2	Ar–Ar	Total rock	Buchely et al. (2009)
DV–165	Granitoide	5° 46' 04.80"	76° 14' 56.40"	43.8 ± 0.8	U–Pb	Zircon	Montes et al. (2015)
DV–167	Granitoide	5° 46' 15.24"	76° 14' 51.00"	42.5 ± 1.3	U–Pb	Zircon	Montes et al. (2015)

Table 4. Radiometric ages of different Chocó–Panamá Arc units (updated from Gómez et al., 2015b and Geología Regional y Prospección Ltd., 2014a, 2014b, 2014c) (*continued*).

Sample	Lithology	Latitude N	Longitude W	Age (Ma)	Dating method	Material analyzed	Reference
			Napi Tonalite				
BX61	Hornblendic diorite	2° 29' 24.04"	77° 28' 52.79"	39 ± 2	K–Ar		McCourt et al. (1990)
HCP10	Hornblendic quartz tonalite	2° 27' 49.62"	77° 30' 00.51"	41 ± 4	K–Ar		McCourt et al. (1990)
JCM3504	Hornblendic gabbro	2° 31' 44.11"	77° 26' 47.97"	43 ± 0.4	K–Ar		McCourt et al. (1990)
BX60	Hornblendic tonalite	2° 29' 31.95"	77° 29' 07.54"	44 ± 4	K–Ar		McCourt et al. (1990)
AM2602	Hornblendic tonalite	2° 31' 10.78"	77° 25' 53.86"	53 ± 5	K–Ar		McCourt et al. (1990)
			Guapi Ultramafite				
APO0056	Diorite/granodiorite	2° 44' 32.22"	77° 14' 26.14"	46.8 ± 0.7	U–Pb LA–ICP–MS	Zircon	Geología Regional y Prospección Ltd. (2014a, 2014b, 2014c)
CLM–0376 R	Granodiorite	2° 30' 33.05"	77° 25' 02.48"	45.6 ± 0.6	U–Pb LA–ICP–MS	Zircon	Geología Regional y Prospección Ltd. (2014a, 2014b, 2014c)
			El Salto Pluton				
BX68	Moscovitic pegmatite	2° 12' 23.81"	77° 39' 30.20"	51 ± 1	K–Ar		McCourt et al. (1990)
			Balsitas Pluton				
BX73	Andesite dike	2° 10' 24.66"	77° 41' 42.43"	42.6 ± 1.3	K–Ar		McCourt et al. (1990)
BX74	Tonalite	2° 10' 24.07"	77° 41' 24.67"	48 ± 1	K–Ar		McCourt et al. (1990)
			Mandé Porphyry Units				
UAKA 80–23	Porphyritic dacite	6° 41' 50.10"	76° 29' 47.93"	42.7 ± 0.9	K–Ar	Hydrothermal sericite	Sillitoe et al. (1982)
WR–238	Porphyritic tonalite	6° 43' 35.7"	76° 31' 16.9"	44.6 ± 0.9	U–Pb LA–MC–ICP–MS	Zircon	Leal–Mejía (2011)
WR–237	Porphyritic tonalite	6° 43' 24.40"	76° 31' 07.40"	45.3 ± 1.2	U–Pb LA–MC–ICP–MS	Zircon	Leal–Mejía (2011)
IGM–900005	Porphyritic andesite	8° 36' 53.01"	77° 21' 44.32"	48.1 ± 2.0	Ar–Ar	Total rock	Present study
UAKA 79–42	Porphyritic tonalite	7° 02' 50.12"	76° 44' 47.95"	54.7 ± 1.3	K–Ar	Hornblende	Sillitoe et al. (1982)
			Porphyry units (South segment)				
BX20R	Andesitic porphyry	2° 12' 44.36"	77° 41' 35.96"	51.5 ± 1.5	K–Ar		McCourt et al. (1990)
AM2586	Andesitic porphyry	2° 17' 14.44"	77° 38' 10.96"	48.4 ± 4.8	K–Ar		McCourt et al. (1990)

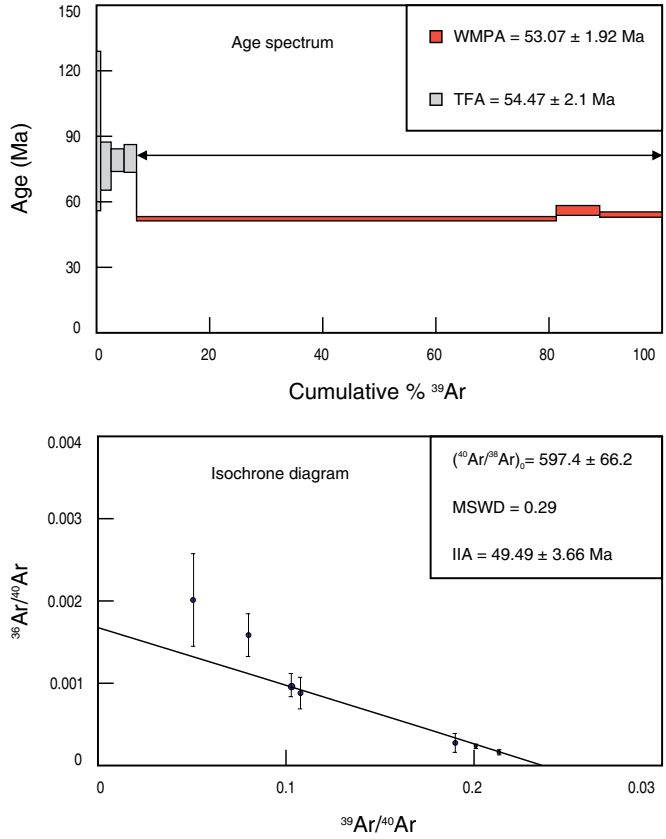

Figure 14. Sample IGM–706477 age range, Mandé Batholith tonalite.

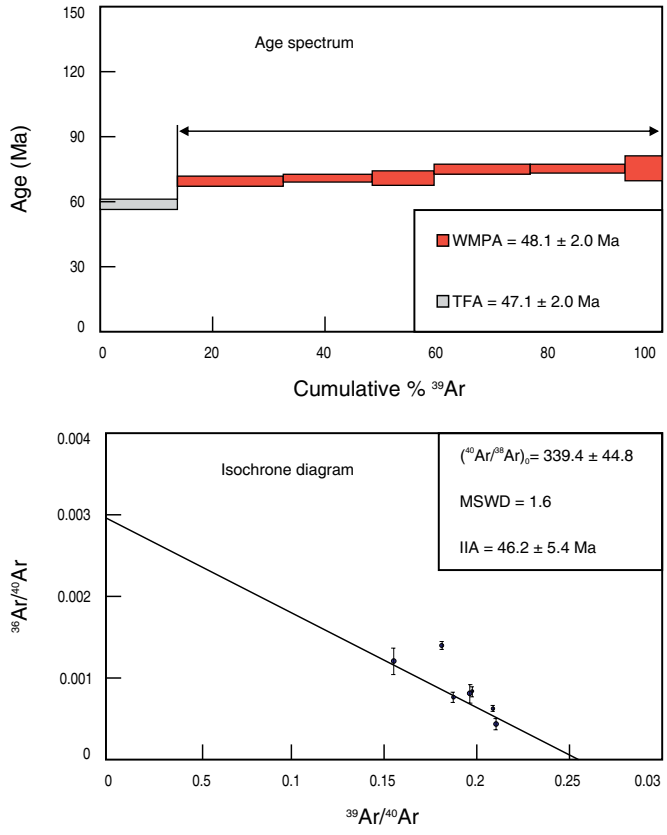

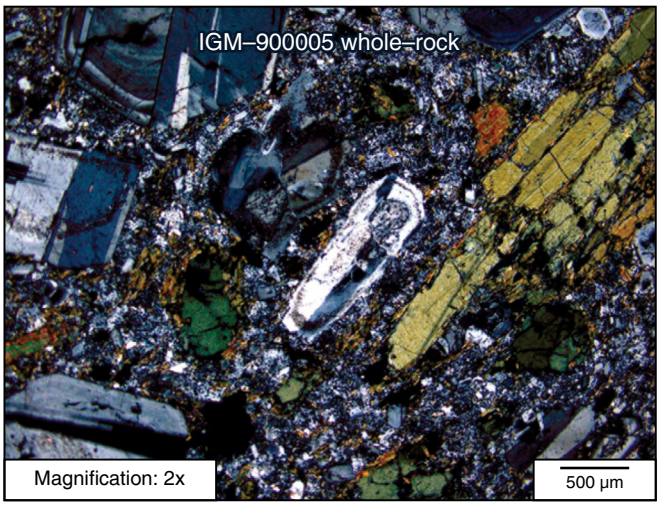

Figure 15. Sample IGM–900005 age range, porphyritic andesite of andesite units and porphyritic dacite.

Urama Diabase (Rodríguez & Arango, 2013) or the Cañasgordas Block (González, 2001) is limited by the Uramita, Dabeiba–Pueblo Rico, and Avirama Faults (Rodríguez & Zapata, 2012), and the basement on which the arc formed is unknown. In the South segment, the eastern boundary with the Dagua Structural Complex is Piedramadura Fault (Geología Regional y Prospección Ltd., 2014a, 2014b, 2014c), under which the arc basement is unknown.

Four samples of basalt and subalkaline tholeiitic diabase (corresponding to basalts with ophitic and subophitic textures composed of crisscrossed plagioclase crystals, clinopyroxene and intersertal glass) distributed along the western edge of the Santa Cecilia–La Equis Complex in the Central segment of the arc present SiO_2 contents between 45.5 and 50.8%, flat REE patterns (similar to those of the San Jose de Urama Diabase), and $(La/Yb)_n$ ratios between 1 and 2. Samples plot within the oceanic basalt field (MORB–OIB), grouped in an intermediate position and outside the Gorgona Basalt and the Colombia Plateau (San José de Urama Diabase) fields. These data may suggest that the arc is built on rocks of oceanic affinity, with different geochemical compositions from the Colombia Plateau and Gorgona Basalt (Table 5, Figure 16).

Echeverri et al. (2015) considered that the Timbiquí Formation and granitoids of arc affinity may be related to the southeastern segment of the Caribbean Plate, including the Panamá Isthmus and the northwest sector of the Colombian continental margin. This area includes a basaltic substrate with plateau affinity and a superimposed magmatic arc <70 Ma. Therefore, the interaction with South America may have lasted from late Eocene to Miocene and may not be related to the rocks of the Colombian Western Cordillera, which would already have been accreted.

This geological context is similar to that of western and central Panamá, where the pre–Oligocene volcanic fronts are emplaced within and on top of the oceanic plateau sequences interpreted to belong to the Caribbean Large Igneous Province (Buchs et al., 2010; Montes et al., 2012). This similarity is consistent with our hypothesis that the pre–Oligocene volcanic front in Panamá and the studied sequences in western Colombia originally belonged to a single intraoceanic volcanic arc.

These four representative data from the oceanic basement where the Chocó–Panamá Arc formed suggest a T–MORB oceanic crust different from the Colombia Plateau of the Western Cordillera. The Chocó–Panamá Arc originally formed as an island arc that later evolved into a continental margin arc (Figure 17) and collided with the western margin of the Colombia Plateau between 37 and 12 Ma. This age range corresponds to the ending of the magmatic activity associated with the Chocó–Panamá Arc and the origin of El Botón Arc, between 12 and 8.5 Ma (Rodríguez & Zapata, 2012; Zapata & Rodríguez, 2011). This latter event intruded the rocks of the Chocó–Panamá Arc and Colombia Plateau. The collision is recorded by the deposi-

Table 5. Trace element values for four diabase and basalt samples with affinity to oceanic crust from the Santa Cecilia–La Equis Complex.

IGM	Latitude N	Longitude W	Sc	Be	V	Cr	Co	Ni	Cu	Zn	Ga	Ge	Rb	Sr	Y	Zr	Nb	In	Sn	Sb	Cs	Ba	La	Ce	Pr	Nd	Sm	Eu	Gd	Tb	Dy	Ho	Er	Tm	Yb	Lu	Hf	Ta	W	Tl	Bi	Th	U
95885	5° 56' 40.00"	76° 15' 10.49"	46	0.5	287	278	42	119	193	118	13	1.6	2	108	18	42	2.7	0.1	1	0.4	0.1	44	3.1	7.5	1.2	6.2	2.1	0.8	2.5	0.5	3.3	0.7	2.1	0.3	2	0.3	1.4	0.2	0.3	0	0.1	0.2	0.1
95888	5° 58' 15.76"	76° 14' 41.22"	46	0.5	271	111	38	83	253	95	17	1.4	5	487	18	55	3	0.1	0.5	0.1	0.1	123	3.3	8.2	1.3	7.3	2.4	1	2.8	0.5	3.4	0.7	2.1	0.3	1.9	0.2	1.7	0.2	0.3	0.1	0	0.2	0.1
700337	5° 49' 41.25"	76° 14' 09.55"	49	0.5	293	369	45	107	121	76	13	1.4	1	103	17	47	2.7	0.1	0.5	0.1	0.1	24	6	12	1.5	6.9	2	0.7	2.5	0.5	3.2		1.9	0.3	1.9	0.3	1.9	0.2	0.5	0.1	1	0.3	0.1
703317	6° 26' 17.87"	76° 20' 10.56"	36	0	175	570	37	240	40	60	10	1	4	132	14	45	1.5	0	0	0.9	0	94	2.7	6.8	1.2	5.9	1.7	0.6	2.3	0.4	2.5	0.5	1.5	0.2	1.4	0.2	1.2	0.1	0	0	0	0.2	0.1

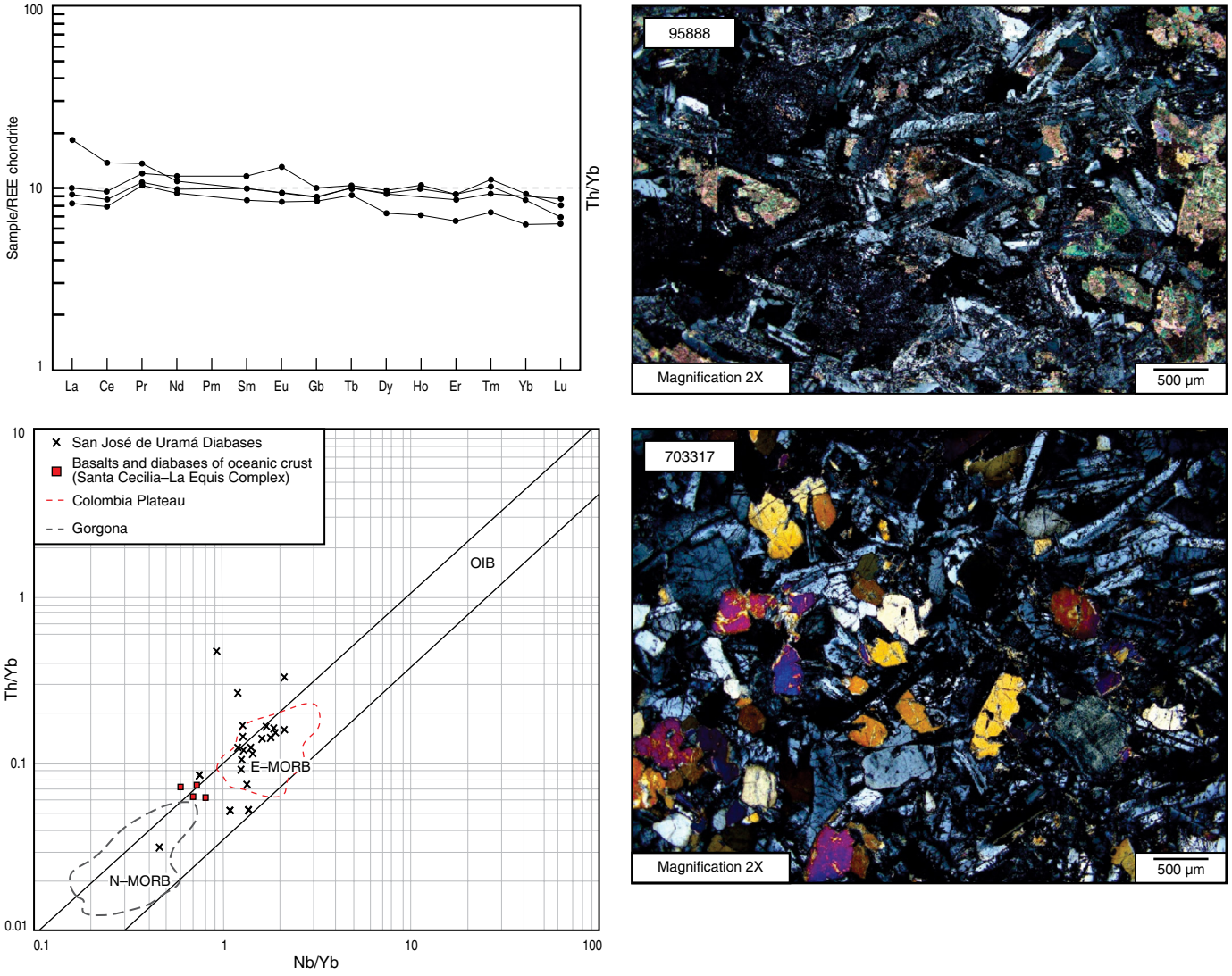

Figure 16. Spider chart of rare earth elements vs. Nakamura chondrite (Nakamura, 1974) and Pearce (2008) oceanic crust rock discrimination diagram for rocks with oceanic affinity in the Santa Cecilia–La Equis Complex, Central segment, and microscopic appearance of samples IGM–95888 and IGM–703317.

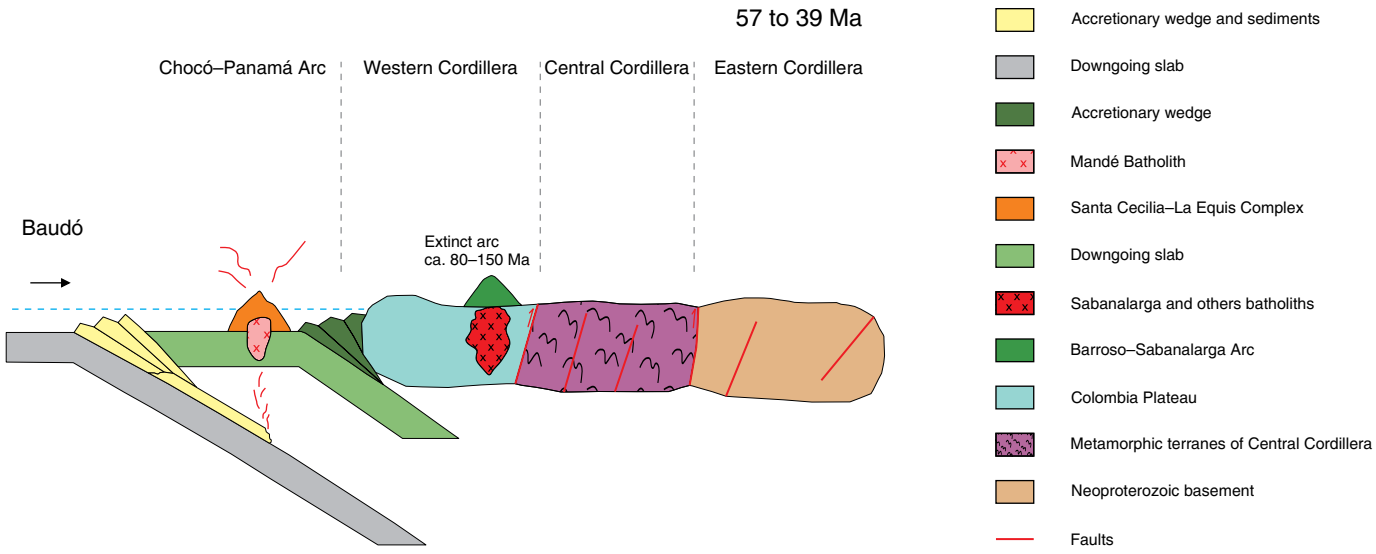

Figure 17. Evolutionary model of the Chocó–Panamá Arc.

tion of units such as the Triganá Breccias (Rodríguez & Sierra, 2010) in the North segment and the Guineales Formation (Rodríguez et al., 2016) in the Central segment.

Acknowledgments

We thank the Servicio Geológico Colombiano, for supplying data used in this study for petrographic analysis, lithogeochemistry, and radiometric dating. Such data were collected by several generations of geologists during projects in the Western Cordillera. We also thank the geologists Francy Helena ORTIZ for generating several figures for this manuscript and Diego RAMÍREZ for helping edit the text in English. We further thank David BUCHS and Diego VILLAGÓMEZ for the comments and corrections made to the manuscript.

References

Álvarez, E. & González, H. 1978. Memoria explicativa: Geología y geoquímica del cuadrángulo I–7 Urrao. Ingeominas, Internal report 347 p. Medellín.

Álvarez, E. & Parra, E. 1979. Evaluación del prospecto de cobre y molibdeno en las cabeceras del río Muerto, municipio de Acandí, departamento del Chocó. Proyecto Col–76/030. Ingeominas–Naciones Unidas, Internal report 1799, 203 p. Medellín.

Annells, R.N., Forero, H.F. & Rodríguez, C.A. 1988. Geology and gold potencial of the Timbiqui and Napi River Basins, Cauca Department, Colombia. Ingeominas–British Geological Survey, Technical Report WC/88/45, 99 p. Nottingham.

Arboleda, G., Celada, C., Forero, S., Montealegre, V., Padilla, J.C., Carmona, J. & Medina, E. 2009. Cartografía geológica y muestreo geoquímico en la parte norte de la cordillera Occidental, planchas 165 y 185 (396 km^2). Contrato n.° 392 de 2007. Ingeominas–UTAGS–GE, unpublished report, 178 p. Bogotá.

Aspden, J.A. 1984. The geology of the Western Cordillera and Pacific coastal plain in the Department of Valle del Cauca (sheets 261, 278, 279, 280 and 299). Ingeominas–Misión Británica (British Geological Survey), Internal report 1959, 61 p. Cali.

Barat, F., Mercier de Lépinay, B., Sosson M., Müller C., Baumgartner P.O. & Baumgartner–Mora, C. 2014. Transition from the Farallon Plate subduction to the collision between South and Central America: Geological evolution of the Panamá Isthmus. Tectonophysics, 622:145–167. https://doi.org/10.1016/j.tecto.2014.03.008

Barrero, D. 1979. Geology of the central Western Cordillera, west of Buga and Roldanillo, Colombia. Publicaciones Geológicas Especiales del Ingeominas, 4:1–75 p. Bogotá.

Botero, G. 1975. Edades radiométricas de algunos plutones colombianos. Revista Minería, 27(169–178): 8336–8342. Medellín.

Buchely, F., Parra, E., Castillo, H., González, F., Dávila, C. & Romero, O. 2009. Realización de la cartografía geológica y muestreo geoquímico en las planchas 144, 145, 128, 129, 113 y 114 (1580 km^2). Contrato n.º 390 de 2007. Ingeominas–GRP, unpublished report, 172 p. Bogotá.

Buchs, D.M., Arculus, R.J., Baumgartner, P.O., Baumgartner–Mora, C. & Ulianov, A. 2010. Late Cretaceous arc development on the SW margin of the Caribbean Plate: Insights from the Golfito, Costa Rica, and Azuero, Panamá, complexes. Geochemistry, Geophysics, Geosystems, 11(7): 35 p. https://doi.org/10.1029/2009GC002901

Calle, B. & Salinas, R. 1986. Memoria explicativa: Geología y geoquímica de la plancha 165 Carmen de Atrato. Scale 1:100 000. Ingeominas, 140 p. Medellín.

Condie, K.C. & Kröner, A. 2013. The building blocks of continental crust: Evidence for a major change in the tectonic setting of continental growth at the end of the Archean. Gondwana Research, 23(2): 394–402. https://doi.org/10.1016/j.gr.2011.09.011

Correa, T., Zapata J.P., Rincón, A.V., Obando, M.G., Ortiz, F.H. & Rodríguez, G. 2017. Edades U–Pb y Ar–Ar obtenidas durante la cartografía 1:50 000 del borde occidental de la plancha 130 Medellín Occidental. XVI Congreso Colombiano de Geología. Memoirs, p. 1223–1228. Santa Marta.

Cossio, U. 1994. Memoria explicativa: Mapa geológico generalizado del departamento del Chocó; geología, recursos minerales y amenazas geológicas. Ingeominas, Internal report 2176, 44 p. Medellín.

Duque–Caro, H. 1990. El Bloque del Chocó en el noroccidente suramericano: Implicaciones estructurales, tectonoestratigráficas y paleogeográficas. Boletín Geológico, 31(1): 47–71. Bogotá.

Echeverri, S., Cardona, A., Pardo–Trujillo, A., Borrero, C., Rosero, S. & López, S. 2015. Correlación y geocronología Ar–Ar del basamento cretácico y el relleno sedimentario Eoceno superior–Mioceno (Aquitaniano inferior) de la cuenca de antearco de Tumaco, SW de Colombia. Revista Mexicana de Ciencias Geológicas, 32(2): 179–189.

Etayo–Serna, F., Barrero, D., Lozano, H., Espinosa, A., González, H., Orrego, A., Ballesteros, I., Forero, H., Ramírez, C., Zambrano–Ortiz, F., Duque–Caro, H., Vargas, R., Núñez, A., Álvarez, J., Ropaín, C., Cardozo, E., Galvis, N., Sarmiento, L., Alberts, J.P., Case, J.E., Singer, D.A., Bowen, R.W., Berger, B.R., Cox, D.P. & Hodges, C.A. 1983. Mapa de terrenos geológicos de Colombia. Publicaciones Geológicas Especiales del Ingeominas, 14(1): 1–135. Bogotá.

Frost, B.R. & Frost, C.D. 2008. A geochemical classification for feldspathic igneous rocks. Journal of Petrology, 49(11): 1955–1969. https://doi.org/10.1093/petrology/egn054

Frost, B.R. & Lindsley, D.H. 1991. The occurrence of iron–titanium oxides in igneous rocks. In: Lindsley, D.H. (editor), Oxide Minerals: Petrologic and Magnetic Significance. Mineralogical Society of America, Reviews in Mineralogy 25: 433–468.

Frost, B.R., Barnes C.G., Collins, W.J., Arculus, R.J., Ellis, D.J. & Frost, C.D. 2001. A geochemical classification for granitic rocks. Journal of Petrology, 42(11): 2033–2048. https://doi.org/10.1093/petrology/42.11.2033

Geología Regional y Prospección Ltd. 2014a. Memoria explicativa: Plancha 318 Bubuey–319 Micay. 395 p. Bogotá.

Geología Regional y Prospección Ltd. 2014b. Memoria explicativa: Plancha 341 El Plateado. 436 p. Bogotá.

Geología Regional y Prospección Ltd. 2014c. Memoria explicativa: Plancha 363 Argelia. 434 p. Bogotá.

Gómez, J., Montes, N.E., Nivia, Á. & Diederix, H., compilers. 2015. Geological Map of Colombia 2015. Scale 1:1 000 000. Servicio Geológico Colombiano, 2 sheets. Bogotá. https://doi.org/10.32685/10.143.2015.936

Gómez, J., Montes, N.E., Alcárcel, F.A. & Ceballos, J.A. 2015b. Catálogo de dataciones radiométricas de Colombia en ArcGIS y Google Earth. In: Gómez, J. & Almanza, M.F. (Editores), Compilando la geología de Colombia: Una visión a 2015. Servicio Geológico Colombiano, Publicaciones Geológicas Especiales 33: 63–419. Bogotá.

González, H. 2001. Memoria explicativa: Mapa Geológico del departamento de Antioquia. Scale 1:400 000. Ingeominas, 240 p. Medellín.

González, H. & Londoño, A.C. 2002. Catálogo de unidades litoestratigráficas de Colombia: Batolito de Mandé, cordillera Occidental. Ingeominas, 19 p. Bogotá.

Guarín, G. & Álvarez, E. 1975. Geología y geoquímica de los prospectos de pórfido cuprífero en el área de Murindó (sectores La Rica, Jarapetó y Táparos), municipio de Riosucio, departamento del Chocó. Ingeominas, Internal report 1738, 105 p. Medellín.

Hansen, J., Skjerlie, K.P., Pedersen, R.B. & De La Rosa, J. 2002. Crustal melting in the lower parts of island arcs: An example from the Bremanger Granitoid Complex, west Norwegian Caledonides. Contributions to Mineralogy and Petrology, 143(3): 316–335. https://doi.org/10.1007/s00410-001-0342-5

Hastie, A.R., Kerr, A.C., Pearce, J.A. & Mitchell, S.F. 2007. Classification of altered volcanic island arc rocks using immobile trace elements: Development of the Th–Co discrimination diagram. Journal of Petrology, 48(12): 2341–2357. https://doi.org/10.1093/petrology/egm062

Hughes, C.J. 1972. Spilites, keratophyres, and the igneous spectrum. Geological Magazine, 109(6): 513–527. https://doi.org/10.1017/S0016756800042795

Ingeominas & Organización de las Naciones Unidas. 1982. Mineralización de cobre y molibdeno en el municipio de Acandí, departamento del Chocó. Unpublished report, DP/UN/COL–76–030/1, 65 p. Bogotá.

Irvine, T.N. & Baragar, W. 1971. A guide to the chemical classification of the common volcanic rock. Canadian Journal of Earth Sciences, 8(5): 523–548. https://doi.org/10.1139/e71-055

Kerr, A.C., Marriner, G.F., Tarney, J., Nivia, A., Saunders, A.D., Thirlwall, M.F. & Sinton, C.W. 1997. Cretaceous basaltic terranes in western Colombia: Elemental, chronological and Sr–Nd isotopic constraints on petrogenesis. Journal of Petrology, 38(6): 677–702. https://doi.org/10.1093/petrology/38.6.677

Leal–Mejía, H. 2011. Phanerozoic gold metallogeny in the Colombian Andes: A tectono–magmatic approach. Doctoral thesis, Universitat de Barcelona, 989 p. Barcelona.

Le Bas, M.J., Le Maitre, R.W., Streckeisen, A. & Zanetin, B. 1986. A chemical classification of volcanic rocks based on the total alkali–silica diagram. Journal of Petrology, 27(3): 745–750. https://doi.org/10.1093/petrology/27.3.745

Le Maitre, R.W., Streckeisen, A., Zanettin, B., Le Bas, M.J., Bonin, B., Bateman, P., Bellieni, G., Dudek, A., Efremova, S., Keller, J., Lameyre, J., Sabine, P.A., Schmid, R., Sørensen, H. & Woolley, A.R., editors. 2002. Igneous rocks: A classification and glossary of terms. Recommendations of the International Union of Geological Sciences Subcommission on the systematics of igneous rocks. Cambridge University Press, 236 p. Cambridge, UK. https://doi.org/10.1017/CBO9780511535581

McCourt, W.J., Muñoz, C.A. & Villegas, H. l990. Regional geology and gold potential of de Guapi–Napi drainage basin and upper Timbiquí River, Cauca Department, SW Colombia. British Geological Survey & Ingeominas, unpublished report, WC/90/34, 241 p. Cali.

Middlemost, E.A.K. 1985. Magmas and magmatic rocks. An Introduction to igneous petrology. Longman Ltd, 266 p. London, New York.

Middlemost, E. A. K. 1994. Naming materials in magma/igneous rock system. Earth–Science Reviews, 37(3–4): 215–224. https://doi.org/10.1016/0012-8252(94)90029-9

Molnar, P. & Sykes, L.R. 1969. Tectonics of the Caribbean and Middle America regions from focal mechanisms and seismicity. Geological Society of America Bulletin, 80(9): 1639–1684. http://dx.doi.org/10.1130/0016-7606(1969)80[1639:TOTCAM]2.0.CO;2

Montes, C., Bayona, G., Cardona, A., Buchs, D.M., Silva, C.A., Morón, S., Hoyos, N, Ramirez, D.A., Jaramillo, C.A & Valencia, V. 2012. Arc–continent collision and orocline formation: Closing of the Central American seaway. Journal of Geophysical Research: Solid Earth, 117(B4): 25 p. https://doi.org/10.1029/2011JB008959

Montes, C., Cardona, A., Jaramillo, C., Pardo, A., Silva, J.C., Valencia, V., Ayala, C., Pérez–Ángel, L.C., Rodríguez–Parra, L.A., Ramírez, V. & Niño, H. 2015. Middle Miocene closure of the Central American Seaway. Science, 348(6231): 226–229 p. https://doi.org/10.1126/science.aaa2815

Nakamura, N. 1974. Determination of REE, Ba, Fe, Mg, Na and K in carbonaceous and ordinary chondrites. Geochimica et Cosmochimica Acta, 38(5): 757–775. https://doi.org/10.1016/0012-8252(94)90029-9

Nelson, W.H. 1962. Contribución al conocimiento de la cordillera Occidental, sección carretera Cali–Buenaventura. Boletín Geológico, 10(1–3): 81–108.

Nivia, A. 1996. El Complejo Estructural Dagua, registro de deformación de la provincia litosférica oceánica cretácica occidental en un prisma acrecionario. VII Congreso Colombiano de Geología. Memoirs, 3, p. 54–67. Bogotá.

Nivia, A. 1998. Memoria explicativa: Mapa geológico del departamento del Valle. Scale 1:250 000. Ingeominas, Internal report 2320, 111 p. Cali.

Nivia, A. 2001. Memoria explicativa: Mapa geológico del departamento del Valle del Cauca. Scale 1:250 000. Ingeominas. 148p. Bogotá.

Parra, E. 1983. Geología y geoquímica de la plancha 223 El Cairo, Valle. Ingeominas, Internal report 1914, 138 p. Medellín.

Pearce, J.A. 1996. User's guide to basalt discrimination diagrams. In: Wyman D.A. (editor), Trace element geochemistry of volcanic rocks: Applications for massive sulphide exploration. Geological Association of Canada, short course notes, 12: p. 79–113. Winnipeg, Canada.

Pearce, J.A. 2008. Geochemical fingerprinting of oceanic basalts with applications to ophiolite classification and the search for Archean oceanic crust. Lithos, 100(1–4): 14–48. https://doi.org/10.1016/j.lithos.2007.06.016

Pearce, J.A., Harris, N.B.W. & Tindle, A.G. 1984. Trace element discrimination diagrams for the tectonic interpretation of granitic rocks. Journal of Petrology, 25(4): 956–983. https://doi.org/10.1093/petrology/25.4.956

Peccerillo, A. & Taylor, S.R. 1976. Geochemistry of Eocene calc–alkaline volcanic rocks from Kastamonu area, northern Turkey. Contributions to Mineralogy and Petrology, 58(1): 63–81. https://doi.org/10.1007/BF00384745

Pindell, J.L. 1993. Regional synopsis of Gulf of Mexico and Caribbean evolution. In: Pindell, J.L. & Perkins, B.F. (editors), Mesozoic and Early Cenozoic Development of the Gulf of Mexico and Caribbean Region: A Context for Hydrocarbon Exploration. Gulf Coast Section SEPM Foundation, 13th Annual Research Conference, p. 251–274. Houston, Texas. https://doi.org/10.5724/gcs.92.13.0251

Pindell, J.L. & Kennan, L. 2009. Tectonic evolution of the Gulf of Mexico, Caribbean and Northern South America in the mantle reference frame: An update. In: James, K.H., Lorente, M.A. & Pindell, J.L. (editors), The origin and evolution of the Caribbean Plate. Geological Society of London, Special Publication 328, p. 1–55. https://doi.org/10.1144/SP328.1

Pindell, J.L., Cande, S.C., Pittman III, W.C., Rowley, D.B., Dewey, J.F., Labrecque, J. & Haxby, W. 1988. A plate–kinematic framework for models of Caribbean evolution. Tectonophysics, 155(1–4): 121–138. https://doi.org/10.1016/0040-1951(88)90262-4

Pindell, J.L., Kennan, L., Maresch, W.V., Stanek, K.P., Draper, G. & Higgs, R. 2005. Plate kinematics and crustal dynamics of circum–Caribbean arc–continent interactions: Tectonic controls on basin development in proto–Caribbean margins. In: Avé–Lallemant, H.G. & Sisson, V.B. (editors), Caribbean–South American Plate interactions: Constraints from the Cordillera de La Costa Belt, Venezuela. Geological Society of America, Special Paper 394, p. 7–52. https://doi.org/10.1130/0-8137-2394-9.7

Ramírez, O., Arias, A., Alminas, H.V. & Mosier, E.L. 1979. Estudio geoquímico en el área Pantanos–Pegadorcito, municipios de Frontino y Dabeiba, Antioquia. Boletín Geológico, 22(2): 53–98. Bogotá.

Ramírez, D.A., Foster, D.A., Min, K., Montes, C., Cardona, A. & Sadove, G. 2016. Exhumation of the Panamá basement complex and basins: Implications for the closure of the Central American seaway. Geochemistry, Geophysics, Geosystems, 17(5): 1758–1777. https://doi.org/10.1002/2016GC006289

Restrepo, J.J. & Toussaint, J.F. 1989. Terrenos alóctonos en los Andes colombianos: Explicación de algunas paradojas geológicas. V Congreso Colombiano de Geología. Memoirs 1: 92–107. Bucaramanga.

Rodríguez, G. & Arango, M.I. 2013. Formación Barroso: Arco volcánico toleítico y diabasas de San José de Urama: Un prisma acrecionario T–MORB en el segmento norte de la cordillera Occidental de Colombia. Boletín Ciencias de la Tierra, (33): 17–38.

Rodríguez, G. & Sierra, M.I. 2010. Las Sedimentitas de Tripogadí y las Brechas de Triganá: Un registro de volcanismo de arco, corrientes de turbidez y levantamiento rápido Eoceno en el noroccidente de Sur América. Geología Colombiana, (35): 74–86.

Rodríguez, G. & Zapata, G. 2012. Características del plutonismo Mioceno superior en el segmento norte de la cordillera Occidental e implicaciones tectónicas en el modelo geológico del noroccidente colombiano. Boletín Ciencias de la Tierra, (31): 5–22.

Rodríguez, G. & Zapata, G. 2013. Análisis comparativo entre la Formación Barroso y el Complejo Quebradagrande: Un arco volcánico toleítico–calcoalcalino, segmentado por el Sistema de Fallas de Romeral en los Andes del norte? Boletín Ciencias de la Tierra, (33): 39–58.

Rodríguez, G., Zapata, G. & Gómez, J.F. 2010a. Geología de la parte oriental de la plancha 114 Dabeiba. Scale 1:100 000. Ingeominas, 175 p. Medellín.

Rodríguez, G., Sierra, M.I., Zapata, G., Correa, T. & Peláez J.R. 2010b. Memoria explicativa: Geología de las planchas 58 Sapzurro (Capurganá), 68 Acandí y 79 bis Unguía (cerro Tagarí). Scale 1:100 000. Ingeominas, 245 p. Medellín.

Rodríguez, G., Arango, M.I. & Bermúdez, J.G. 2012. The Sabanalarga Batholith, arc plutonism in the suture zone between continental and oceanic crust in the northern Andes. Boletín Ciencias de la Tierra, (32): 81–98.

Rodríguez, G., Zapata, G. & Gómez, J.F. 2013. Memoria explicativa: Geología de la plancha 114 Dabeiba. Scale 1:100 000. Ingeominas, 211 p. Medellín.

Rodríguez, G., Arango, M.I., Zapata, G. & Bermúdez, J.G. 2016. Estratigrafía, petrografía y análisis multi–método de procedencia de la Formación Guineales, norte de la cordillera Occidental de Colombia. Boletín de Geología, 38(1): 101–124. https://doi.org/10.18273/revbol.v38n1-2016006

Salazar, G., James, M. & Tistl, M. 1991. El Complejo Santa Cecilia–La Equis: Evolución y acreción de un arco magmático en el norte de la cordillera Occidental, Colombia. Simposio de magmatismo andino y su marco tectónico. Memoirs, (2): 142–160. Manizales.

Salazar, G., González, L.M., Muñoz, R., Güiza, S. & Moreno, G. 2005. Caracterización de unidades litogeoquímicas de la cordillera

Occidental: Fase I, plancha 165. Ingeominas, unpublished report, 58 p. Bogotá.

Serrano, L., Ferrari, L., López Martínez, M., Maria Petrone, C., Jaramillo, C. 2011. An integrative geologic, geochronologic and geochemical study of Gorgona Island, Colombia: implications for the formation of the Caribbean Large Igneous Province. Earth and Planetary Science Letters, 309(3–4): 324–336. https://doi.org/10.1016/j.epsl.2011.07.011

Shand, S.J. 1943. Eruptive rocks. Their genesis, composition, classification, and their relation to ore deposits, with a chapter on meteorites. John Wiley & Sons, 444 p. New York.

Sillitoe, R.H., Jaramillo, L. Damon, P.E. Shafiqullah, M. & Escobar, R. 1982. Setting, characteristics, and age of the Andean porphyritic copper belt in Colombia. Economic Geology, 77(8): 1837–1850. https://doi.org/10.2113/gsecongeo.77.8.1837

Streckeisen, A. 1976. To each plutonic rock its proper name. Earth–Science Reviews, 12(1):1–33. https://doi.org/10.1016/0012-8252(76)90052-0

Streckeisen, A. 1979. Classification and nomenclature of volcanic rocks, lamprophyres, carbonatites, and melilitic rocks: Recommendations and suggestions of the IUGS Subcommission on the Systematics of Igneous Rocks. Geology, 7(7): 331–335. https://doi.org/10.1130/0091-7613(1979)7<331:-CANOVR>2.0.CO;2

Sun, S.S. & McDonough, W.F. 1989. Chemical and isotopic systematics of oceanic basalts: Implications for mantle composition and processes. In: Saunders, A.D. & Norry, M.J. (editors), Magmatism in the ocean basins. Geological Society of London, Special Publication 42, p. 313–345. https://doi.org/10.1144/GSL.SP.1989.042.01.19

Toussaint, J.F. 1996. Evolución geológica de Colombia: 3 Cretácico. Universidad Nacional de Colombia, 277 p. Medellín.

Villagómez, D.R. 2010. Thermochronology, geochronology and geochemistry of the Western and Central Cordilleras and Sierra Nevada de Santa Marta, Colombia: The tectonic evolution of NW South America. Doctoral thesis, University of Geneva, 126 p. Geneva, Switzerland.

Villagómez, D., Spikings, R., Magna, T., Kammer, A., Winkler, W. & Beltrán, A. 2011. Geochronology, geochemistry and tectonic evolution of the Western and Central Cordilleras of Colombia. Lithos, 125(3–4): 875–896. https://doi.org/10.1016/j.lithos.2011.05.003

Weber, M., Gómez, J., Cardona, A., Duarte, E., Pardo–Trujillo, A. & Valencia, V.A. 2015. Geochemistry of the Santa Fé Batholith and Buriticá Tonalite in NW Colombia–Evidence of subduction initiation beneath the Colombian Caribbean Plateau. Journal of South American Earth Sciences, 62: 257–274. https://doi.org/10.1016/j.jsames.2015.04.002

Wegner, W., Wörner, G., Harmon, R.S. & Jicha, B.R. 2011. Magmatic history and evolution of the Central American Land Bridge in Panamá since Cretaceous times. Geological Society of America Bulletin, 123(3–4): 703–724. https://doi.org/10.1130/B30109.1

Whattam, S.A. & Stern, R.J. 2015. Late Cretaceous plume–induced subduction initiation along the southern margin of the Caribbean and NW South America: The first documented example with implications for the onset of plate tectonics. Gondwana Research, 27(1): 38–63. https://doi.org/10.1016/j.gr.2014.07.011

Wood, D.A. 1980. The application of a Th–Hf–Ta diagram to problems of tectonomagmatic classification and to establishing the nature of crustal contamination of basaltic lavas of the British Tertiary Volcanic Province. Earth and Planetary Science Letters, 50(1): 11–30. https://doi.org/10.1016/0012-821X(80)90116-88

Zapata, G. & Rodríguez, G. 2011. Basalto de El Botón, arco volcánico mioceno de afinidad shoshonítica al norte de la cordillera Occidental de Colombia. Boletín Ciencias de la Tierra, (30): 77–91.

Zapata–Villada, J.P., Restrepo, J.J., Cardona–Molina, A. & Martens, U. 2017. Geoquímica y geocronología de las rocas volcánicas básicas y el Gabro de Altamira, cordillera Occidental (Colombia): Registro de ambientes de plateau y arco oceánico superpuestos durante el Cretácico. Boletín de Geología, 39(2): 13–30. https://doi.org/10.18273/revbol.v39n2-2017001

Explanation of Acronyms, Abbreviations, and Symbols:

ANH	Agencia Nacional de Hidrocarburos
Ap	Apatite
Bt	Biotite
Cal	Calcite
Chl	Chlorite
Cpx	Clinopyroxene
Ep	Epidote
Hbl	Hornblende
HFSE	High field strength element
HREE	Heavy rare earth element
ICP–MS	Inductively coupled plasma mass spectrometry
Kfs	Potassium feldspar
LA–ICP–MS	Laser ablation inductively coupled plasma mass spectrometry
LILE	Large ion lithophile element
LOI	Loss on ignition
LREE	Light rare earth element
MALI	Alkali–lime index
Ms	Muscovite
MSWD	Mean square weighted deviation
N–MORB	Normal mid–ocean ridge basalts
OIB	Oceanic island basalts
Ol	Olivine
Op	Opaque
Opx	Orthopyroxene
Phnocr	Phenocrystals
Pl	Plagioclase
QAFP	Quartz, Alkali feldspar, Plagioclase
Qtz	Quartz
REE	Rare earth element
RF	Rock fragments
SGC	Servicio Geológico Colombiano
STP	Standard temperature and pressure
TAS	Total alkali silica
T–MORB	Transitional mid–ocean ridge basalts
Tr	Trace elements
Tr–Act	Tremolite–Actinolite
Ttn	Titanite
Zrn	Zircon

Authors' Biographical Notes

Gilberto ZAPATA–GARCÍA graduated with a degree in mining and geological engineering from the Russian State Geological Prospecting University (Российский государственный геологоразведочный университет) (MGRI–RSGPU) in 1977 and specialized in urban–regional planning at the Universidad Nacional de Colombia, Sede Medellín in 2000. He worked in geological mapping at a scale of 1:100.000, exploration, and petrography at Servicio Geológico Colombiano, from 1978 to 2017. Since 2014, he has been a member of the Proyecto Estudios Geológicos Especiales, participating in studies on Jurassic magmatism in Colombia.

Gabriel RODRÍGUEZ–GARCÍA graduated in 1987 with a degree in geological engineering from the Universidad Nacional de Colombia, Sede Medellín. Subsequently, he completed specialization studies at the École Nationale Supérieure des Mines de Paris in 1995, specializing in technical evaluation–economics of mining projects. He has worked for 30 years at the Servicio Geológico Colombiano. He was the head of cartography of the regional headquarters of Ibagué, and acts as coordinator of projects and regional cartography and of work groups for the exploration and evaluation of deposits. He currently coordinates the Medellín headquarters and the Grupo de Estudios Geológicos Especiales of the Servicio Geológico Colombiano. He has previously been a professor of Colombian Geology, Field Geology I, and Physical Geology at Universidad EAFIT and the director of geology of Grupo Argos. He has authored over 100 publications, including geological maps, memoirs, and scientific articles in geology.